Aus dem Institut für Klinische Radiologie

der Ludwig-Maximilians-Universität München

Direktor: Prof. Dr. med. Dr. h.c. Maximilian Reiser, FACR, FRCR

Dual Energy Computertomographie – Objektive Dosimetrie, Bildqualität und Dosiseffizienz

Dissertation

zum Erwerb des Doktorgrades der Medizin

an der Medizinischen Fakultät der

Ludwig Maximilians-Universität zu München

vorgelegt von

Jan Christian Schenzle

aus Essen

München 2012

Mit Genehmigung der Medizinischen Fakultät der Universität München

Berichterstatter:	Priv. Doz. Dr. Thorsten Johnson
Mitberichterstatter:	Priv. Doz. Dr. Thomas Pfluger
	Prof. Dr. Karl Schneider
Dekan:	Prof. Dr. med. Dr. h.c. M. Reiser, FACR, FRCR
Tag der mündlichen Prüfung:	24.05.2012

Kumulative Dissertation Gemäß § 4a der Promotionsordnung

Inhaltsverzeichnis

1. Einleitung und Grundlagen

Schon früh nach Entdeckung der materiedurchdringenden Strahlung durch Wilhelm Conrad Röntgen im Jahr 1895 erkannte man ihre enorme Bedeutung für die diagnostische Medizin. In den folgenden einhundert Jahren erlebte die Entwicklung von Röntgengeräten, die in der Lage waren, mit hochenergetischer Strahlung „undurchsichtiges“ Körpergewebe zu durchleuchten, einen rasanten Fortschritt – ausgehend von den konventionellen Schattenbildern der frühen Tage bis hin zur heutigen hochauflösenden Computertomografie in 3D. Die vielfältigen Möglichkeiten der Röntgenuntersuchungen sind aus dem klinischen Alltag heute nicht mehr wegzudenken, aber es gab bereits im Jahr 1896, nach der anfänglichen Euphorie über diese neuartige Diagnosemöglichkeit in der Medizin, Zweifel an der „Harmlosigkeit“ der neuen Strahlen für den Menschen. Auf die gewebeschädigenden Nebenwirkungen der ionisierenden Strahlung wurde man erst aufmerksam, als sich medizinischen Komplikationen bei bestrahlten Patienten einstellten. Durch die konsequente technische Weiterentwicklung der Röntgen-Technologie konnte jedoch die Strahlenbelastung im Laufe der Zeit ganz erheblich gesenkt werden bei gleichzeitiger Steigerung der Bildqualität.

Die Forderung, für die Behandlung von Patienten eine qualitativ hochwertige Diagnostik mit geringstmöglicher Strahlenbelastung im Bereich der Schnittbildverfahren zur Verfügung zu stellen, wurde durch die kontinuierliche Weiterentwicklung neuer Generationen von Computer-Tomographen, adaptiver Kollimatorsysteme sowie dosissparender Benutzersoftware realisiert. Heute machen CT-Untersuchungen ca. 7% aller durchgeführten Röntgenuntersuchungen aus, sind jedoch für ca. 54 % der verabreichten effektiven Gesamtdosis verantwortlich.[1]

Somit sind Bedenken von Patienten wie auch die Zurückhaltung von Spezialisten der Radiologie gegenüber derartigen Untersuchungen durchaus angebracht; dies gilt insbesondere für neuentwickelte und bisher noch nicht im Detail etablierte Untersuchungsprotokolle. [2, 3] Andererseits lassen sich viele wichtige klinische Fragestellungen aufgrund der erforderten hohen zeitlichen und räumlichen Auflösung nur mit Hilfe der CT beantworten.

In den vorliegenden Studien wurden sogenannte Dual Source Computer-tomographen verwendet, welche grundsätzlich über drei verschiedene Betriebsarten verfügen. Zum einen kann das Gerät mit nur einer Röntgenquelle wie ein normaler Computertomograph betrieben werden. Die beiden anderen Betriebsarten benötigen dagegen zwei Röntgenquellen, welche innerhalb einer Gantry um 90° versetzt angeordnet sind. Werden beide Quellen mit der gleichen Spannung betrieben, kann eine deutliche Reduktion der Aquisitionszeit und damit eine effektive Reduktion von Bewegungsartefakten beispielsweise bei kardiologischen Untersuchungen erreicht werden, da für die Datenaquisition einer Schicht lediglich eine Rotation von 90° statt 180° benötigt wird. Bei der Beurteilung von Herzkranzgefäßen auch bei höheren oder arrhythmischen Herzfrequenzen lassen sich durch dieses Verfahren störende Bewegungsartefakte vermeiden, sodass es im Bereich der Akutmedizin mittlerweile als gängiges Verfahren etabliert ist. Außerdem kann der Tischvorschub (Pitch) so stark erhöht werden, dass beide Spiralpfade ineinander laufen, wodurch eine sehr viel schnellere Volumenabdeckung erreicht wird. Das „Triple-Rule-Out“ Protokoll beispielsweise bietet die Möglichkeit, bei Patienten mit akuten thorakalen Beschwerden drei Differenzialdiagnosen, der Myokardinfarkt, die Aortendissekation

sowie die Lungenarterienembolie, in einer einzigen Untersuchung mit hoher Präzision, relativ niedriger Dosis und geringem zeitlichen Aufwand zu unterscheiden.

Die Dual Source Technologie bietet neben den „High-Pitch“ Protokollen eine weitere Anwendungsmöglichkeit. Im sogenannten Dual Energy Modus werden die vorhandenen Röntgenquellen mit unterschiedlichen Spannungspotenzialen betrieben und ermöglichen durch die Energieabhänginkeit der Photonenwechselwirkungen von Compton- und Photoeffekt eine Differenzierung des Materials aufgrund der unterschiedlichen Massenschwächungskoeffizienten und der Kernladungszahl des untersuchten Gewebes. [4] Durch das unterschiedliche Absorptionsverhalten verschiedener Gewebearten können somit durch eine aufwändige Nachverarbeitung einzelne Gewebearten identifiziert und voneinander getrennt werden. Ein kleiner Auszug aus den vielfältigen Anwendungsbereichen sind z.B. die Trennung von Iod und Knochenmaterial, Nieren- oder Gallengangssteindifferenzierung, die Jodverteilung bei Lungenperfusions-Untersuchungen oder beispielsweise die Erkennung von koronaren Plaques. [5-24]

Die erste Studie im Rahmen dieser Promotionsarbeit mit dem Titel „Dual Energy CT of the Chest – How about the dose?“ [25] wurde an zwei verschiedenen Computertomographen, dem Siemens Somatom Definition sowie dem Nachfolgemodell Siemens Somatom Definition Flash durchgeführt. Beide Geräte verfügen über die Möglichkeit, mittels Röntgenquellen unterschiedlicher Betriebsspannung (Dual Energy) Spektralaufnahmen anzufertigen. Diese bieten je nach klinischer Fragestellung z.B. im Bereich der pulmonalen Durchblutungssituation bei Lungenarterienembolien nützliche Zusatzinformationen im Vergleich zu einer standardmäßigen CT-Angiografie.

Einschränkungen der Bildqualität ergaben sich aufgrund der bisher verwendeten Betriebsspannungen von 140kVp/80kVp insbesondere in Bereichen hoher Absorption wie z.B. Schulter- und Beckengürtel, aber auch bei Untersuchungen des Abdomens adipöser Patienten, sodass eine dickere Kollimation auf Kosten der Bildqualität benötigt wurde, um dosisneutrale Schnittbilder im Vergleich zur Standard CTA zu erzeugen. Um das Problem der hohen Absorption zu lösen, wurde zur besseren Strahlentransmission die Betriebsspannung der zweiten Röntgenquelle auf 100kVp erhöht, wodurch eine feinere Kollimation mit 0.6 mm verwendet werden konnte. Hierdurch vergrößerte sich jedoch die Überlappung der Röntgenspektren von Röhre 1 und 2, was jedoch den Vorteil der spektralen Gewebedifferenzierung reduzierte. Erst durch die Verwendung eines Zinn-Filter-Systems im Gerät der zweiten Generation konnte eine Reduktion des Niedrigenergiespektrums der Röntgenröhre höherer Spannung (140kVp) erreicht werden, die zu einer deutlichen Verbesserung des spektralen Kontrasts führte. Ziel der vorliegenden Studie war eine objektive Quantifizierung der effektiven Äquivalentdosis von Dual Energy CT Untersuchungen unter realen Bedingungen und deren Vergleich zu einer konventionellen computertomographischen Untersuchung.

Die zweite Studie im Rahmen dieser Promotionsarbeit mit dem Titel „Saving Dose in Triple-Rule-Out-CT using a High-Pitch Dual Spiral Technique" [26] behandelt eine Thematik der Akutmedizin. Bei Patienten mit akuten Thoraxschmerzen, welche derzeit ca. 7 % der Vorstellungen in einer internistischen Notaufnahme ausmachen, hat sich die Anwendung eines Triple-Rule-Out Protokolls zur simultanen Beurteilung von Lungenarterien, Koronararterien sowie Dissekationen der Hauptschlagader vereint in einer einzelnen Untersuchung, etabliert. Die offensichtlichen Vorteile dieser bildgebenden Methode führten zu einer Zunahme solcher Untersuchungen bei

Patienten mit akutem Thoraxschmerz. Bisher verwendete Protokolle arbeiteten zur suffizienten Datenaquisition mit einem Tischvorschub von 0.2 bis 0.4 (Pitch), bedingt durch Einflussfaktoren wie Geschlecht, Herzfrequenz sowie dem gewählten Verfahren zu EKG-synchonisierten Aufnahmetechnik. Damit verbunden war die Aufnahme von überlappenden Spiralen, was zu einer erhöhten effektiven Strahlendosis führte. Die Verwendung von Dual Source Computertomographen für solche Untersuchungen hat es nun durch Nutzung der zusätzlichen Röntgenquelle innerhalb einer Gantry mit der gleichen Betriebsspannung (120kVp) möglich gemacht, deutlich höhere Pitch-Werte zu verwenden. Die schnellere Rohdatenaquisition resultiert in einer Reduktion von Bewegungsartefakten insbesondere im Bereich der Koronararterien, sodass Untersuchungen ohne Überlappung mit befriedigendem Ergebnis möglich werden. Ziel dieser Studie war die Ermittlung der effektiven Strahlendosis der Untersuchungsmethode im Vergleich zu Routine-Protokollen.

2. Methodik

Zur Quantifizierung der benötigten Effektivdosis der beiden unterschiedlichen Verfahren wurde in Zusammenarbeit mit dem Bundesamt für Strahlenschutz des Helmholtz-Zentrums München ein anthropomorphes Alderson-Rando-Phantom ausgewählt, dessen Messpunkte innerhalb des Phantoms mit Thermo-Lumineszens-Detektoren (TLD) bestückt wurden. Dieses Messprinzip ist als objektives und universelles Dosimetrie-Verfahren etabliert. Hierbei war eine detaillierte Einarbeitung in das Thema der medizinischen Dosimetrie, Datengewinnung und Interpretation essentiell für die Planung und Durchführung des technischen Teils der Studien.

Hauptteil der messtechnischen Arbeit bestand nach der Erstellung der Studienplanung in der Aufteilung der Einzel-Messpunkte (n = 58) auf repräsentative Bereiche (Region of interest, ROIs), in der Bestückung des Phantoms mit den einzelnen Detektoren (TLD), der Durchführung des Scan-Vorgangs unter Verwendung der verschiedenen Protokoll-Typen sowie des Auslese-Prozesses der Detektoren zur Datengewinnung. Die so erhaltenen Rohdaten wurden mittels eigens entwickelten Algorithmen unter Verwendung organspezifischer Wichtungsfaktoren nach ICRP-103 innerhalb des Untersuchungsgebiets zu kumulativen Effektivdosen summiert. Somit konnte nach Interpretation der erhaltenen Messergebnisse eine Aussage bezüglich der effektiven Strahlenbelastung und Bildbeurteilbarkeit (SNR, CNR) der einzelnen verwendeten Untersuchungsmethoden getroffen und die Strahlenbelastung, Bildqualität sowie das Kontrastverhältnis im Vergleich zu bisherigen Standarduntersuchungen beurteilt werden.

2.1 Alderson Rando Phantom

Beide vorliegenden Studien wurden an einem sogenannten Alderson-Rando-Phantom (Alderson Research Inc. Stanford) durchgeführt. Dieses repräsentiert einen 175 cm großen, 73,5 kg schweren männlichen Patienten und wird unter anderem vom Bundesamt für Strahlenschutz des Helmholtz-Zentrums München zur Kontrolle der Einhaltung des Strahlenschutz-Gesetzes für in Deutschland zugelassene Röntgengeräte verwendet.

2.2 Computertomographie-Protokolle

In den vorliegenden Studien wurden für die verschiedenen Fragestellungen unterschiedliche Aquisitionsprotokolle verwendet und verglichen. Für die Gewinnung der Dual Energy Datensätze wurden Röhrenspannungen von 140/80kVp sowie Sn140/100 kVp ausgewählt und mit einem Standard 120kVp Thoraxprotokoll verglichen. Die Datengewinnung des High-Pitch Protokolls erfolgte mit einer 2 x 120kVp Röhrenspannung und wurde mit dem oben genannten Standard 120kVp Protokoll sowie einem retrospektiv EKG-getriggerten konventionellen Thoraxschmerz-Protokoll verglichen. Zusätzlich wurde eine definierte Scanlänge von 276 mm für alle verwendeten Untersuchungsmethoden zur exakten Vergleichbarkeit verwendet.

2.3 Thermolumineszenz -Detektor

Zur objektiven Dosismessung wurden 58 Thermolumineszenz-Detektoren verwendet. Dieses Verfahren wird seit langem im Bereich der Strahlentherapie zur Quantifizierung der applizierten Strahlendosis und somit zur Therapieüberwachung eingesetzt. Hauptbestandteil des Detektors ist ein mit Magnesium und Titan dotierter Lithium-Fluoridkristall, welcher bei Bestrahlung mit hochenergetischen Photonen Elektronen emittiert und innerhalb der Kristallstruktur einfängt. Diese Elektronen repräsentieren die applizierte Dosis und können durch einen optischen Prozess in Form eines charakteristischen Glühkurvenverlaufs in einem geeigneten TL-Detektor ausgelesen werden. Die einzelnen Detektoren wurden in repräsentativen Bereichen wie z.B. Lunge, Knochenmark, Leber innerhalb sowie an der Oberfläche (Haut) des Alderson-Phantoms platziert.

2.4 Dosisberechnung

Zur Quantifizierung der Einzeldosen in Bezug auf die bestrahlten Bereiche konnte unter Verwendung von organspezifischen Wichtungsfaktoren nach ICRP 103 die individuelle effektive Strahlenbelastung der einzelnen Organe errechnet und somit eine Aussage zur kumulativen Gesamtdosis der verschiedenen verwendeten Untersuchungsmethoden getroffen werden.

2.5 Bildbeurteilbarkeit

Um eine Aussage bezüglich der Bildqualität der einzelnen Protokolle treffen und diese untereinander vergleichen zu können, wurden die Rohdatensätze unter Verwendung der identischen Faltungskerne (D30f) rekonstruiert und die Standardabweichungen an 14 verschiedenen Regionen (ROI) innerhalb des Phantoms registriert und untereinander verglichen. Bei Kontrastmittel-gestützten Untersuchungen wie beispielsweise das Thoraxschmerz-Protokoll ist zusätzlich das Verhältnis von Kontrast zu Bildrauschen von großem Interesse. Hierfür wurden Flüssigkeitsbehälter mit jodhaltigem Kontrastmittel sowie einer 0,9% Natriumchlorid-Lösung in einem errechneten Mischungsverhältnis, ähnlich der Blut-Jod-Konzentration während Kontrastmittelaufnahmen, unter Verwendung der einzelnen Protokolle untersucht.

2.6 Ergebnisse

Für die Dosismessung der ersten Studie „Dual Energy oft the chest – How about the dose“ ergab sich für das Sn 140/100 kVp Protokoll eine effektive Dosisbelasung von 2,69 mSv sowie 2,61 mSV für das 140/80 kVp Protokoll im Vergleich zur Standarduntersuchung im 120 kVp Protokoll mit 2,70 mSV. Das gemessene Bildrauschen ergab nach statistischer Analyse mittels ANOVA keinen signifikanten Unterschied ($p = 0.342$). Unter Verwendung eines nichtlinearen Blending-Algorithmus (Optimum Contrast) ergab sich ein 128 % besserer Kontrast : Rausch (CNR) Verhältnis für die Dual Energy Protokolle im Vergleich zum Standard 120 kVp Protokoll.

Die zweite vorliegende Studie „Saving Dose in Triple-Rule-Out-CT using a High-Pitch Dual Spiral Technique” ergab mit 2,65 mSV im Vergleich zum retrosektiv EKG-getriggerten Chestpain-Protokoll mit 19,27 mSv eine deutlich geringere Strahlenbelastung bei nicht-signifikant unterschiedlichen Bildrauschwerten und somit gleichwertiger Bildbeurteilbarkeit.

3. Zusammenfassung

Der Hintergrund der beiden vorliegenden Studien war eine objektive Betrachtung neuentwickelter Methoden der modernen bildgebenden Diagnostik hinsichtlich der Strahlenbelastung für den menschlichen Organismus. Mit der Einführung der Dual Source Computertomographen eröffnete sich ein weites Spektrum an neuen diagnostischen Möglichkeiten. Durch den simultanen Betrieb der um 90° versetzt angeordneten Röntgenquellen lassen sich bewegungsartefaktfreie Schichtaufnahmen mit hoher zeitlicher und räumlicher Auflösung erzeugen, welche der

schnellen Ursachendiagnostik im Bereich der Akutmedizin bei Thoraxschmerz-Patienten zu Gute kommt. Der Dual Energy Modus, in welchem die Röntgenquellen mit unterschiedlichen Energien betrieben werden, erlaubt eine Materialdifferenzierung, was eine Unterscheidung von beispielsweise Knochen, Jod oder anderen organischen Materialien ermöglicht. [6-17] Dass diese technischen Neuerungen einen weiteren wertvollen Beitrag zur klinischen Diagnostik leisten können, steht angesichts der vielfältigen Einsatzmöglichkeiten außer Frage. Es galt jedoch nachzuweisen, dass diese neuen Verfahren nicht zu einer zusätzlichen Strahlenbelastung im Vergleich zu den bisher verwendeten Methoden zu Lasten der untersuchten Patienten führen. Durch die Verwendung eines anthropomorphen Phantoms und geeigneter Detektoren konnten die resultierenden Strahlenbelastungen der unterschiedlichen Untersuchungsprotokolle auf den menschlichen Organismus quantifiziert werden. Für die Durchführung der Dual Energy Protokolle konnte im Vergleich zu den standardmäßigen Computertomographie-Untersuchungen eine Dosisneutralität bei vergleichbarer Bildqualität und deutlich verbessertem Kontrast-zu-Rausch Verhältnis nachgewiesen werden. Das Dual Energy Protokoll kommt heute unter anderem routinemäßig bei Patienten mit klinischem Verdacht auf eine Pulmonalarterien-Embolie zur Anwendung.

Ein wichtiger Erfolg in Bezug auf die Dosiseinsparung konnte durch die Einführung des Triple-Rule-Out Protokolls erreicht werden. Hierbei lassen sich nun unterschiedliche Fragestellungen aus der Akutmedizin bei Patienten mit akutem Thoraxschmerz wie Myokardinfarkt, Lungenarterienembolie oder Aortendissekation, in einer einzigen Untersuchung mit hoher Präzision und einem Bruchteil der bisher benötigten Strahlendosis beantworten.

4. Abstract

The aim of the present studies was an objective reflection of newly developed methods of modern imaging techniques concerning radiation exposure to the human body. Dual Source computed tomography has opened up a broad variety of new diagnostic possibilities. Using two X-ray sources with an angular offset of about 90° in a single gantry, images with a high spatiotemporal resolution can be achieved, for example in patients suffering acute chest pain . The Dual Energy Mode is based on the acquisition of two data sets with two different x-ray spectra which make it possible to identify certain substances with different spectral properties like bone, iodine or other organic material. [6-17] There is no doubt that this technical innovation will make an essential contribution to clinical diagnostics, but it remained to be proven that there is no additional dose.

An anthropomorphic Phantom and thermoluminiscent detectors were used to objectively quantify the radiation dose resulting from the different examination protocols.

For Dual Energy CT examinations, it was possible to verify dose neutrality in combination with comparable image quality and even improved contrast to noise ratio. Nowadays, this protocol is used in clinical routine examinations, e.g. for the evaluation of pulmonary embolism.

A milestone in dose reduction was reached with modern triple rule out protocols. Causes of acute chest pain such as heart attack, pulmonary embolism or aortic rupture can be differentiated in a single examination with a high precision and a fractional amount of dose compared to conventional methods.

Dual Energy CT of the Chest

How About the Dose?

Jan C. Schenzle, Wieland H. Sommer, MD,* Klement Neumaier,† Gisela Michalski,† Ursula Lechel, MS,‡ Konstantin Nikolaou, MD,* Christoph R. Becker, MD,* Maximilian F. Reiser, MD,* and Thorsten R. C. Johnson, MD**

Objective: New generation Dual Source computed tomography (CT) scanners offer different x-ray spectra for Dual Energy imaging. Yet, an objective, manufacturer independent verification of the dose required for the different spectral combinations is lacking. The aim of this study was to assess dose and image noise of 2 different Dual Energy CT settings with reference to a standard chest scan and to compare image noise and contrast to noise ratios (CNR). Also, exact effective dose length products (E/DLP) conversion factors were to be established based on the objectively measured dose.

Materials and Methods: An anthropomorphic Alderson phantom was assembled with thermoluminescent detectors (TLD) and its chest was scanned on a Dual Source CT (Siemens Somatom Definition) in dual energy mode at 140 and 80 kVp with 14 × 1.2 mm collimation. The same was performed on another Dual Source CT (Siemens Somatom Definition Flash) at 140 kVp with 0.8 mm tin filter (Sn) and 100 kVp at 128 × 0.6 mm collimation. Reference scans were obtained at 120 kVp with 64 × 0.6 mm collimation at equivalent CT dose index of 5.4 mGy*cm. Syringes filled with water and 17.5 mg iodine/mL were scanned with the same settings. Dose was calculated from the TLD measurements and the dose length products of the scanner. Image noise was measured in the phantom scans and CNR and spectral contrast were determined in the iodine and water samples. E/DLP conversion factors were calculated as ratio between the measured dose form the TLDs and the dose length product given in the patient protocol.

Results: The effective dose measured with TLDs was 2.61, 2.69, and 2.70 mSv, respectively, for the 140/80 kVp, the 140 Sn/100 kVp, and the standard 120 kVp scans. Image noise measured in the average images of the phantom scans was 11.0, 10.7, and 9.9 HU ($P > 0.05$). The CNR of iodine with optimized image blending was 33.4 at 140/80 kVp, 30.7 at 140Sn/100 kVp and 14.6 at 120 kVp. E/DLP conversion factors were 0.0161 mSv/mGy*cm for the 140/80 kVp protocol, 0.0181 mSv/mGy*cm for the Sn140/100 kVp mode and 0.0180 mSv/mGy*cm for the 120 kVp examination.

Conclusion: Dual Energy CT is feasible without additional dose. There is no significant difference in image noise, while CNR can be doubled with optimized dual energy CT reconstructions. A restriction in collimation is required for dose-neutrality at 140/80 kVp, whereas this is not necessary at 140 Sn/100 kVp. Thus, CT can be performed routinely in Dual Energy mode without additional dose or compromises in image quality.

Key Words: dual energy CT, radiation exposure, image noise, contrast to noise ratio, lung perfusion

(*Invest Radiol* 2010;45: 000–000)

Received September 20, 2009; accepted for publication (after revision) January 19, 2010.

From the *Departments of Clinical Radiology, and †Radiotherapy and Radiooncology, University Hospitals-Grosshadern, Ludwig-Maximilians University, Munich, Germany; and ‡Federal Office for Radiation Protection, Department of Medical Radiation Hygiene and Dosimetry Helmholtz-Zentrum, Neuherberg, Germany.

The authors J. C. S. and W. H. S. contributed equally to the study.

Reprints: Thorsten R. C. Johnson, MD, Department of Clinical Radiology, University of Munich, Grosshadern Campus, Marchioninistr 15, 81377 Munich, Germany. E-mail: thorsten.johnson@med.uni-muenchen.de.

ISSN: 0020-9996/10/4506-0001

The rapid advances in computed tomography (CT) continuously improve image quality and diagnostic accuracy. The robustness and speed of the modality entails a wide and growing spectrum of clinical indications. However, the consistently increasing use of ionizing radiation and the growing total dose to the population have triggered concerns about cancer risk and sparked off a trend to new dose-saving techniques.[1] In Germany, CT examinations represent about 7% of all x-ray examinations (2004) but account for more than 54% of the resultant total effective dose.[2] Therefore, any new CT technology that may require an additional radiation exposure has to be regarded with caution.

A new generation of CT scanners integrating 2 x-ray sources and detectors in one gantry with an angular offset of about 90° has increased the temporal resolution by a factor of 2[3,4] and thus brought about a new reliability of cardiac imaging.[5,6] Also, this system design makes spectral imaging, ie, Dual Energy CT (DECT), feasible in clinical routine.[7] This technique is based on the acquisition of 2 CT datasets with 2 different x-ray spectra which are generated with different tube voltages and filters. The images are reconstructed separately from the projection data of both detectors and can be used to identify certain substances with spectral properties, eg, iodine or xenon gas. The imaging data from both detectors can also be averaged into one image, generating a dataset similar to a standard 120 kV acquisition, but this is only possible for the field of view (FOV) covered by both detectors with a maximum coverage of 33 cm diameter. There are multiple applications for DECT, and several studies have shown clinical benefits as the exact identification of renal stones,[8–10] detection and characterization of liver or kidney neoplasm,[11–13] assessment of myocardial perfusion,[14] visualization of lung perfusion or ventilation,[15–18] or bone removal from angiographic datasets.[19–21] Several other fields of application are still being developed and evaluated.

In the early development of DECT, its clinical value was still unclear and an additional radiation exposure not justified. Therefore, DECT protocols were set such that the CT dose index, ie, the dose applied to a certain range, approximately equals that of a normal CT scan of the individual area of the body. To achieve comparable noise levels, the tube currents of both tubes were adapted with a certain relation, because the efficiency in output of x-ray quanta is highly energy dependent.[7] The 80 and 140 kVp are routinely used because these voltages are achievable with the x-ray tubes and generate an adequate difference in attenuation. Still, the spectral difference is limited by the broad overlap of the 2 x-ray spectra (Fig. 1). Moreover, the limited transmission of 80 kVp quanta in dense areas of the body such as the shoulders, the pelvis, or the abdomen requires a thicker collimation if no additional dose is to be administered.[11,22]

A new 0.4 mm thick tin (Sn) filter was implemented in the new version of the Siemens DSCT scanner (Siemens Definition Flash) to rid the 140 kVp spectrum of low-energy quanta and to further separate the spectra so that a similar spectral contrast can be

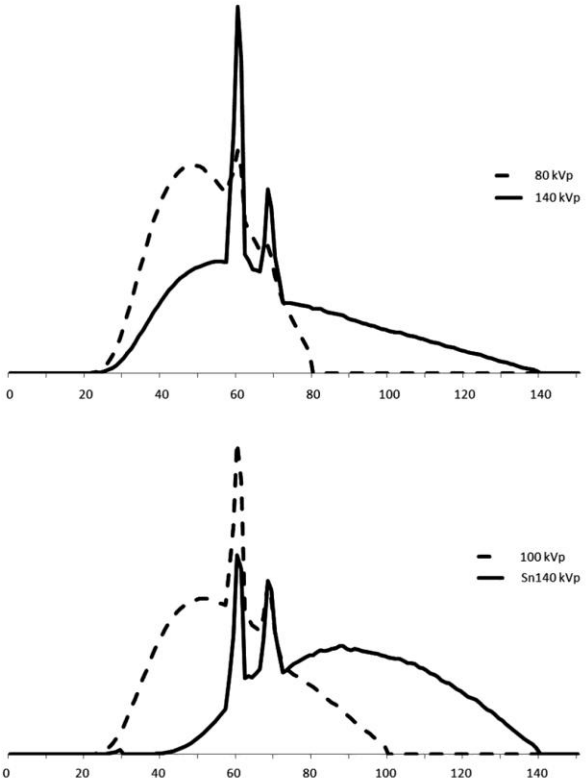

FIGURE 1. Photon energy spectra of the x-ray tubes operating at 80 and 140 kV potential are shown in red and blue, and the spectrum of a tube running at 140 kVp with additional 0.4 mm tin filter (SPS, selective photon shield) shown in green. Note the significantly smaller overlap between the 80 and Sn140 kVp spectra (Source of Monte Carlo simulation data: Siemens Healthcare, Forchheim, Germany).

obtained with a combination of the filtered Sn-140 kVp and a 100 kVp spectrum.[23] Thus, insufficient transmission of thin 80 kVp projections in large or dense objects such as the abdomen is avoided, and a thin 0.6 mm collimation can be used.

The purpose of this study was to assess dose and image noise of different DECT protocols in manufacturer independent, objective measurements with thermoluminescent dosimeters, compared with a standard pulmonary CT angiography scan for reference. Additionally, the contrast to noise ratio (CNR) of spectral information was to be determined with different combinations of x-ray spectra using iodine and water samples. A further purpose was to assess the performance of nonlinear blending algorithms, which are useful to optimize contrast information in CT images derived from DECT. Furthermore, exact effective dose length products (E/DLP) conversion factors were to be established based on the objective dose information from the thermoluminescent detectors (TLD).

Overall, the question to be answered was, whether DECT requires additional dose compared with conventional CT or not, also taking compromises in collimation or image noise into account.

FIGURE 2. Scan range for the chest, covering the entire lungs and mediastinum, the lower neck, the domes of the diaphragms, and a part of the upper abdomen. The scan length in all protocols was kept equal with 276 mm.

MATERIALS AND METHODS

TLD Preparation

For objective dose measurements independent from manufacturer calibration, thermoluminiscent detectors (TLD) were used. The main component of a TLD is a combination of lithium and fluorine doped with magnesium and titanium. When a crystal lattice like lithium and fluorine is irradiated, electrons are emitted and trapped by the impurity of magnesium and titanium. These trapped electrons represent the amount of measured radiation and can be read-out up to 24 hours after exposure without loss of information. TLDs were primarily developed for radiotherapy and are designed to measure radiation in the range of one or several Grays (Gy). To measure dose in TLDs, a complex prearrangement is necessary, including cumulating calibration factors. To generate these factors, each TLD was exposed to exactly 1 Gy using a ^{137}CS source and subsequently read out to obtain the measured TLD dose, standard deviations and its sensitivity.

Alderson Rando Phantom Assembly

The TLDs were placed in an anthropomorphic Alderson-Rando phantom representing a 175 cm tall, 73.5 kg male patient with a thoracic diameter of 32 cm (Alderson Research Laboratories Inc., Stanford, CT). The phantom was equipped with 58 thermoluminescent dosimeters with dimensions of 1 × 1 × 6 mm (TLD-100H, Bicron Harshaw, Radiation Measurement Products, Cleveland, OH). Each TLD position was carefully selected in the region of interest for a thoracic scan, considering the scan range and the additional range potentially affected by scatter radiation (Fig. 2). To evaluate specific organ doses and account for z-axis variability for each scan protocol, the TLDs were allocated to every organ in several slices in the scan range:

Lung (n = 14), thyroid gland (n = 1), esophagus (n = 4), vertebral spine (n = 5), mediastinum (n = 4), liver (n = 6), stomach (n = 1) colon (n = 1), and skin (n = 22).

TLD Exposure

To assess effective radiation dose, E/DLP conversion factors, noise and CNR, the Alderson phantom was scanned on Dual Source CT scanners using 3 different scan protocols:

TABLE 1. CT—Parameter Settings of the Dual Energy and Conventional 120 kVp Chest Protocols

Protocol	Dual Energy Scan Definition	Dual Energy Scan Definition Flash	Standard Chest Scan Definition Flash
Voltage tube A (kVp)	140	100	120
Voltage tube B (kVp)	80	Sn140	
Reference current-time product tube A (mAs)	80	165	160
Reference current-time product tube B (mAs)	340	140	
Effective current-time product tube A (mAs)	30	73	90
Effective current-time product tube B (mAs)	117	68	
CT dose index with CareDose4D (mGy)	5.37	5.37	5.89
Scan length (mm)	276	276	276
Pitch	0.7	0.55	1.2
Gantry rotation time (sec)	0.5	0.28	0.5
Collimation (mm)	14 × 1.2	128 × 0.6	128 × 0.6
Reconstructed slice thickness/position increment (mm)	2	2	2
Kernel	D30f	D30f	D30f

1. Dual Energy pulmonary CT angiography protocol at 140/80 kVp.
2. Dual Energy pulmonary CT angiography protocol at Sn140/100 kVp.
3. Single Energy pulmonary CT angiography protocol at 120 kVp.

Detailed scan parameters are listed in Table 1. The first protocol was performed on a Dual Source CT (Siemens Somatom Definition, Forchheim, Germany) in dual energy mode at 140 and 80 kVp with 14 × 1.2 mm collimation. The same was applied on a second generation Dual Source CT scanner (Siemens Somatom Definition Flash, Forchheim, Germany) at 140 kVp with 0.4 mm tin filter (Sn) and 100 kVp at 128 × 0.6 mm collimation. Reference scans were obtained at 120 kVp with 128 × 0.6 mm collimation at equivalent volume CT dose index (pitch corrected CTDIvol) of 5.4 mGy*cm, also on the Definition Flash scanner. To compare dose efficiency, the same dose was to be applied with all 3 protocols. To achieve a higher total radiation exposure and to minimize statistical variations, all scan protocols were repeated 10 times with constant parameter settings. Therefore, the tube current was adjusted such that the user interface showed a CTDIvol of 5.4 mGy*cm.

TLD Read-Out

To read out the TLD after exposure, each Rod was heated to 350 centigrade using a nitrogen flow. With heating, the trapped electrons in the TLD emit a characteristic glow curve when switching their atomic energy level. This is detected by a photomultiplier and converted to the specific amount of absorbed radiation. The read out procedure consisted of the following steps:

1. Sorting TLD to a carrier plate.
2. Read-Out process using a TL-Detector 2000D (Harshaw Radiation Measurement Products, Cleveland, OH) to generate specific glow curves and a TL Picoprocessor 2080 (Harshaw) to convert to dose.
3. TLD Storage deletion using a TLDO Annealing Oven (PTW, Freiburg, Germany).

Dose Calculation

Dose was calculated from the TLD measurements and the appropriate organ weighting factors,[24] and specific conversion coefficients were calculated from the dose length products of the scanner.

The overall dose was calculated from the individual doses of the TLDs in one organ. The effective dose of the chest was calculated by multiplying the sum of the absorbed organ dose with its appropriate tissue weighting factor according to ICRP-103.[24] Lung, esophagus, and mediastinum are fully covered in the scan range and their dose was entirely taken into account. At the ends of the scan range, the partial coverage of the individual organ in the scan range was taken into account by estimating the exposed share of the organ in relation to its total size. Several organs in the scan area including the heart, the mediastinal lymph nodes, the pararenal glands, and the pancreas, are not assigned to a specific conversion factor in ICRP-103[24] but are summed in the "remainder tissues" parameter which also contains several other organs. We estimated a share of 40% of these organs to be exposed. The percentages used for the other organs are listed in Table 2.

E/DLP Conversion Factors

To determinate E/DLP conversion factors X, the measured effective doses (D_E) from the TLDs and the dose length product (DLP) from the patient protocol were divided:

$$X = \frac{D_E(\text{mSv})}{\text{DLP}(\text{mGy} \times \text{cm})}$$

Noise Measurements

Images were reconstructed from every acquisition using a D30f convolution kernel and a slice thickness and increment of 2 mm (Fig. 3). To achieve similar spectral properties, average images were reconstructed from the dual energy CT acquisitions with weighted contributions from both detectors, ie, applying the standard weighting factor of 0.3 to include 70% of density information from the 140 kVp dataset and 30% from the 80 kVp acquisition. With the combination of the filtered 140 kVp and the 100 kVp spectra, average images were reconstructed with equivalent contributions from both detectors, ie, with the standard weighting factor of 0.5. These weighting factors imply a linear blending, ie, every image voxel contains density information from both datasets with a fixed linear relation.

For noise measurements, 14 regions of interest (ROI) at 7 different z-axis positions were chosen inside the phantom in a homogeneous area of the mediastinum. A standardized ROI size of 4.20 cm^2 and equivalent positions were used for all acquired protocols. Noise was calculated for each acquisition protocol as the average standard deviation of CT numbers in all regions of interest.

TABLE 2. TLD Measurement Results With the Corresponding Partial Doses at Current Organs Including the Organ Specific Weighting Factors for All Three Protocols

Measured Dose (mSv)					
Organ	**Definition (140/80 kVp)**	**Definition Flash (Sn140/100 kVp)**	**Standard Chest (120 kVp)**	**Weighting Factor (ICRP103)**	**Share Exposed**
Thyroid gland	0.21	0.27	0.18	0.04	50%
Lung	0.99	0.99	1.06	0.12	100%
Esophagus	0.34	0.33	0.37	0.04	100%
Bone marrow	0.28	0.28	0.30	0.12	33%
Bone surface	0.02	0.02	0.02	0.01	33%
Remainder tissues*	0.41	0.39	0.46	0.12	40%
Liver	0.10	0.10	0.06	0.04	50%
Stomach	0.19	0.23	0.19	0.12	50%
Colon	0.052	0.064	0.045	0.12	20%
Skin	0.014	0.014	0.015	0.01	18%
Total	2.606	2.688	2.700		

*Remainder tissues contain adrenals, extrathoracic (ET) region, gall bladder, heart, kidneys lymphatic nodes, muscle, oral mucosa, pancreas, prostate, small intestine, spleen, thymus, uterus/cervix.

FIGURE 3. Example for density measurements. Two ROIs are placed in a homogeneous area of the phantom's mediastinum.

Contrast to Noise Ratio Measurements

To quantify the CNR, which is more relevant for the diagnostic evaluation than image noise, phantom measurements with iodine and water were performed. Two syringes were filled, one with a mixture of contrast material and saline (concentration 17.5 mg iodine/mL comparable to the concentration in blood in an angiographic examination) and one with saline solution (NaCl 0.9%). The syringes were placed on the chest of the Alderson phantom, surrounded by a water bag with a layer of about 2 cm of water on top of the syringes to limit beam hardening. The different protocols mentioned above were performed with equal settings, and images were reconstructed using the same kernel and slice thickness. Two ROI were measured in the lumen of both syringes at 4 different z-axis positions.

To quantify the CNR, 3 different calculation approaches were used. First, to evaluate general image quality, a general CNR was determined in average images of the dual energy acquisitions and in the standard 120 kVp images. These CNR values were calculated as quotient of the mean value of CT numbers of the contrast material in the syringe and the image noise, ie, its standard deviations.

To evaluate the performance of nonlinear blending algorithms, optimized images were additionally reconstructed using an US Food and Drug Administration approved software (Syngo Dual Energy optimum contrast, Siemens).[25] This software loads both the high and low energy dataset and optimizes contrast and noise in the image. This is achieved by variably adding different relations of density information from both datasets, limiting noise in homogeneous areas with data from the high energy image and improving contrast in areas containing iodine by adding more information from the low energy image. In the resulting images, CNR was determined in the same manner.

Additionally, the spectral contrast in Dual Energy images was determined to quantify the spectral separation. The CNR value was calculated as the difference between the CT numbers in the center of the iodine syringe at Sn140 kVp and 100 kVp, divided by the background noise. The CNR was also calculated for images at 140 kVp and 80 kVp.

Statistics

The significance of differences between noise values or CNR was tested using an analysis of variance (ANOVA). In case of significant results of the ANOVA, posthoc t-tests for unpaired samples were used. In case of multiple comparisons, the *P* value was corrected according to Bonferroni.

RESULTS

Dose Length Products

The dose length products in the patient protocols were 143 mGy*cm for the 140/80 kVp examination on the Somatom Definition, 165 mGy*cm for the Sn140/100 kVp protocol and 146 mGy*cm for the 120 kVp single-source scan on the Somatom Definition Flash. Using a standard conversion factor of 0.017 mSv/mGy*cm[26] for the chest in literature to estimate effective Dose, these values would correspond to 2.43, 2.80, and 2.48 mSv, respectively (Fig. 4).

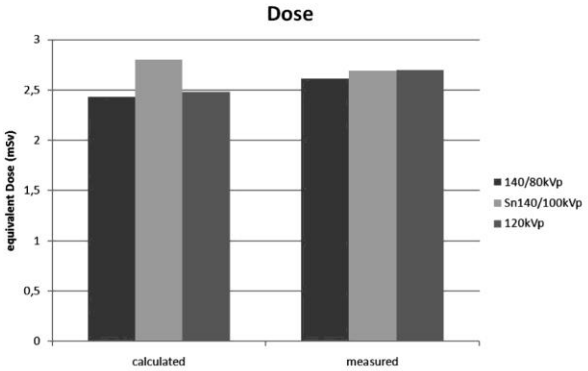

FIGURE 4. Comparison of radiation dose. Calculated doses result from the DLP of the patient protocol multiplied by a standard E/DLP conversion factor for the chest (0.017). Measured dose represent the exact dose, measured by TLDs and summarized taking the tissue weighting factor according to ICRP-103 into account.

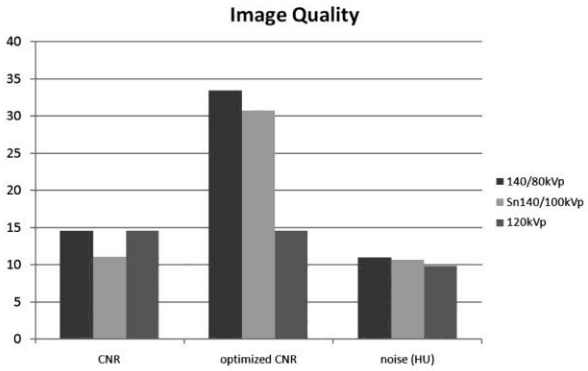

FIGURE 5. Comparison of different image quality measures. CNR values are defined as contrast enhancement divided by background noise. Optimized CNR is achieved with nonlinear blending algorithms, which use dual energy information to enhance the display of contrast material in the image.

Measured Dose

The doses measured in the individual organs with TLDs in the Alderson Rando phantom are listed in Table 2. After multiplication with the organ specific weighting factors according to IRCP 103,[24] the corresponding effective dose amounted to 2.61, 2.69, and 2.70 mSv, respectively, for the 140/80 kVp, the 140 Sn/100 kVp and the standard 120 kVp scan (Fig. 4).

Conversion Factors

As a basis to estimate patient doses as correctly as possible in a clinical setting, E/DLP conversion factors were calculated as ratio between the measured dose and the dose length product given in the patient protocol. The corresponding values were 0.0161 mSv/mGy*cm for the 140/80 kVp protocol, 0.0181 mSv/mGy*cm for the Sn140/100 kVp mode, and 0.0180 mSv/mGy*cm for the 120 kVp examination.

Image Noise

In the average images of the Sn140/100 kVp scan with 0.6 mm collimation reconstructed at 2 mm slice thickness, the image noise amounted to 10.7 HU. The 140/80 kVp scan with a collimation of 14 × 1.2 mm reconstructed with the same kernel and slice thickness resulted in a nearly equal image noise of 11.0 HU. With the standard 120 kVp chest protocol, the resulting noise was slightly lower with an average of 9.9 HU. Statistical analysis, using ANOVA did not reveal any statistically significant differences ($P = 0.342$) between the noise measured with the different protocols.

As noise is inversely related to the square root of dose,[27] an exactly equivalent noise as in the 120 kVp standard examination would require an estimated increase of 7% in dose at 140/80 kVp with 1.2 mm collimation or 11% at Sn140/100 kVp with 0.6 mm collimation.

Contrast to Noise Ratio

The general iodine contrast in the weighted average images was comparable to that in standard 120 kVp images. The corresponding CNR values amounted to 14.6 for the 140/80 kVp protocol, 11.1 for the Sn140/100 kVp protocol, and 14.6 for the 120 kVp scan, ie, there was no difference between the 140/80 kVp and 120 kVp spectra. The statistical analysis using ANOVA resulted in a significantly lower CNR for the Sn140/100 kVp ($P < 0.05$).

With the optimum contrast images which had been generated using the nonlinear blending algorithm, the contrast to noise ratio was considerably better with 30.7 for the Sn140/100 kVp protocol and 33.4 for the 140/80 kVp protocol, ie, 87 and 128% higher than with the standard 120 kVp spectrum ($P < 0.01$; cf. Fig. 5). There was no statistically significant difference between both Dual Energy protocols.

Regarding the spectral contrast, which is important for dual energy post processing, there were expected major differences between the 2 combinations of x-ray spectra. Mean difference in attenuation in the iodine syringe in the Sn140/100 kVp scan was 192 HU with a noise of 25.2 HU, resulting in a contrast to noise ratio of 7.62. The 140/80 kVp scan showed a difference in attenuation of 311 HU with a noise of 26.6 HU, resulting in a CNR of 11.7. The difference between both spectral combinations in CNR was statistically significant ($P < 0.01$).

DISCUSSION

In clinical routine DECT may offer additional, clinically relevant information. Several studies have meanwhile shown the benefits of this new imaging technique in clinical routine using an Food and Drug Administration approved software with several different applications.[7,8,11,15,16,19,28–31] On the other hand, recent publications[1] on lifetime attributable cancer risk of CT examinations have sparked off considerable awareness of radiation exposure,[32] its risks and appropriate indications.

Comparison of Dual Energy Protocols to Standard 120 kVp Chest Protocol

Our study tested 2 different Dual Energy chest protocols and compared them to a conventional 120 kVp protocol. With respect to radiation dose, the Dual Energy protocols resulted in 2.61 mSv and 2.69 mSv for the 140/80 kVp and Sn140/100 kVp, respectively, whereas the standard 120 kVp chest protocol amounted to 2.70 mSv. These objective dose measurements confirmed comparable doses for all 3 protocols. In this phantom study, image noise was not significantly different between these 3 protocols. Regarding CNR values, Sn140/100 kVp setting showed significantly lower values, if using the standard settings. However, these differences were outweighed using the nonlinear blending algorithm.

Comparison of 140/80 kVp and Sn140/100 kVp Setting

As the results for CNR and spectral contrast show, the hardened 140 kVp spectrum in combination with the tin filter and 100 kVp reference spectrum provides a smaller CNR and spectral contrast compared with 140/80 kVp setting. This difference is caused by the larger overlap of the spectra in the former setting and the higher mean energy which results in a loss of photoelectric effect. In contrast, the transmission of photons increases with this setting, which is a benefit for examinations in obese patients. Taking into account that the Alderson Rando phantom is relatively slim compared with the average patient in clinical routine, the advantages of the better transmission of the combination Sn140/100 kVp may not have been fully illustrated by the noise measurements in this study, but are quite evident in our clinical experience. In abdomen and chest, 1.2 mm collimation were used so far to compensate noise in 80 kVp acquisitions which is reflected by high noise using a 0.6 mm collimation in combination with a 140/80 kVp spectra.[8] The new tin filter and the hardened 140 kVp spectrum makes it possible to use 100 kVp as reference spectrum with the side effect of a weaker CNR as reflected in our measurements in iodine and water samples. In this respect, our measurement could not confirm the simulations by Primak et al,[23] from which one could expect an even improved CNR.

The different CT settings like collimation, tube current and reconstructed slice thickness must also be taken into account when comparing image noise between Sn140/100 kVp and 140/80 kVp setting.[33] The collimation applied at Sn140/100kVp protocol was 128 × 0.6 mm, which makes it possible to reconstruct thin slices of 0.6 mm thickness at the price of an increased background noise generated by the detector itself and the subsequent data processing. Practically this results in a difference of 0.8 HU more noise in comparison with a standard 120 kVp chest acquisition. A collimation of 14 × 1.2 mm used at 140/80 kVp scan decreases background noise by pooling the signals of 2 detector elements on one analog/digital converter and thus creates thicker layers.

Clinical Implications

Comparing Dual Energy protocols and standard pulmonary CTA protocols, the diagnostic relevance of an inferior image quality would not necessarily be outweighed by the spectral information, implying that average images should offer a similar quality and dose efficiency as standard CT acquisitions. The diagnostically relevant CNR values using optimized postprocessing imply that at least for angiographic examinations no additional dose is required and that linear blending algorithms can even improve CNR considerably at equivalent dose. This differs from the observations of Ho et al[34] who observed 2- to 3-fold doses for dual energy CT. However, their setup was based on a single source system using rapid voltage switching and contained neither a normalization of image noise nor of dose, so the lower energy spectrum was obtained additionally, whereas the higher energy spectrum was obtained with the same tube current time product as the single energy scan. In contrast, our approach was based on a dual source system with the same CT dose index for single and dual energy scans, so it is not surprising that the dose of the protocols is comparable.

A major problem of the first generation DSCT system is the restriction in FOV to 26 cm diameter which is caused by the geometrical arrangement of the second x-ray tube and the resulting smaller detector. For DECT, this represents a relevant limitation especially in the evaluation of lung perfusion and ventilation or the reconstruction of virtual noncontrast images of kidney and liver lesions.[11,16,22,28] With the design of the Siemens Definition Flash with a larger second detector at an increased angular offset, the 33 cm FOV resolves this limitation very well, because this diameter is sufficient to include the diagnostically relevant organs in most of patients.

The advantage of DECT is that it can offer additional information from a single scan on demand, like specific spectral information on contrast enhancement or an additional "virtual" noncontrast reconstruction.[22] Several studies have shown that, for example, the exact mapping of lung perfusion[29] or ventilation or a differentiation of kidney stones[8] is now feasible and offers clinical advantages without additional dose or limitations in image quality. This practical value only applies if DECT routinely replaces standard protocols, and knowing that the Dual Energy protocols are clinically feasible with comparable radiation dose, they can be used as standard setting for a wide range of applications.

Limitations of the Study

Ideally, noise measurements and CNR comparisons should be performed exactly in the center of the gantry, which is not possible in the Alderson phantom with its antropomorphic anatomy. As we acquired our measurements at equivalent positions with all 3 protocols, the comparison should remain valid. Also, image noise is not homogeneous over the whole FOV but generally decreases in the periphery, which may increase contrast to noise ratio. We did not specifically address this issue with our measurements. Still, as we performed our measurements with the Alderson phantom centered exactly in the gantry for the different scan protocols and identically positioned regions of interest, the comparison should be valid. We also only evaluated syringes with water and iodine in high concentration to determine CNR. From these experiments, conclusions can only be drawn for angiographic examinations in which similar iodine concentrations are achieved in the vessel, but not for other clinical issues such as the detection of focal lesions in solid organs. Another limitation is that we applied different collimations with the different spectral combinations. The simple reason is that the 80 kVp spectrum yields insufficient transmission in average size adult patients with 0.6 mm collimation, while 100 kVp image noise is acceptable with the Sn140/100 kVp combination, and then it is clinically useful to apply the thinner collimation. Thus, our measurements reflect clinically applicable scan parameters with the different spectral combinations.

CONCLUSION

DECT of the chest is feasible without additional dose. There is no significant difference in image noise, while CNR can be doubled with optimized dual energy CT reconstructions. Regarding the total applied dose, the possibility of virtual noncontrast reconstructions can even reduce the dose by a factor of 2 if an unenhanced scan is omitted. With a restricted collimation of 14 × 1.2 mm, 140/80 kVp examinations lead to approximately the same image noise and radiation dose but a higher Dual Energy contrast and CNR compared with 140Sn/100 kVp acquisitions with a finer collimation of 128 × 0.6 mm. Overall, image quality, image noise and dose are comparable to a standard 120 kVp chest protocol, and virtual unenhanced reconstructions and a wide range of specific applications like eg, ventilation or perfusion imaging can be chosen on demand.

REFERENCES

1. Einstein AJ, Henzlova MJ, Rajagopalan S. Estimating risk of cancer associated with radiation exposure from 64-slice computed tomography coronary angiography. *JAMA*. 2007;298:317–323.
2. Lechel U, Becker C, Langenfeld-Jager G, et al. Dose reduction by automatic exposure control in multidetector computed tomography: comparison between measurement and calculation. *Eur Radiol*. 2009;19:1027–1034.

3. Flohr TG, McCollough CH, Bruder H, et al. First performance evaluation of a dual-source CT (DSCT) system. *Eur Radiol*. 2006;16:256–268.
4. Petersilka M, Bruder H, Krauss B, et al. Technical principles of dual source CT. *Eur J Radiol*. 2008;68:362–368.
5. Johnson TR, Nikolaou K, Wintersperger BJ, et al. Dual-source CT cardiac imaging: initial experience. *Eur Radiol*. 2006;16:1409–1415.
6. Johnson TR, Nikolaou K, Busch S, et al. Diagnostic accuracy of dual-source computed tomography in the diagnosis of coronary artery disease. *Invest Radiol*. 2007;42:684–691.
7. Johnson TR, Krauss B, Sedlmair M, et al. Material differentiation by dual energy CT: initial experience. *Eur Radiol*. 2007;17:1510–1517.
8. Graser A, Johnson TR, Bader M, et al. Dual energy CT characterization of urinary calculi: initial in vitro and clinical experience. *Invest Radiol*. 2008; 43:112–119.
9. Scheffel H, Stolzmann P, Frauenfelder T, et al. Dual-energy contrast-enhanced computed tomography for the detection of urinary stone disease. *Invest Radiol*. 2007;42:823–829.
10. Thomas C, Krauss B, Tsiflikas I, et al. Differentiation of urinary calculi with dual energy CT: effect of spectral shaping by high energy tin filtration. *Invest Radiol.* In press.
11. Graser A, Johnson TR, Chandarana H, et al. Dual energy CT: preliminary observations and potential clinical applications in the abdomen. *Eur Radiol*. 2009;19:13–23.
12. Robinson E, Babb J, Chandarana H, et al. Dual source dual energy MDCT: preliminary observations comparing 80 kVp and weighted average 120 kVp data for conspicuity of hypo-vascular liver metastases. *Invest Radiol.* In press.
13. Graser A, Staehler M, Macari M, et al. Single-phase dual energy CT allows for characterization of renal masses as benign or malignant. *Invest Radiol.* In press.
14. Zhang L, Peng J, Wu SY, et al. Dual source dual energy CT of acute myocardial infarction: correlation with histopathological findings in a canine model. In press.
15. Chae EJ, Seo JB, Goo HW, et al. Xenon ventilation CT with a dual-energy technique of dual-source CT: initial experience. *Radiology*. 2008;248:615–624.
16. Thieme SF, Becker CR, Hacker M, et al. Dual energy CT for the assessment of lung perfusion—correlation to scintigraphy. *Eur J Radiol*. 2008;68:369–374.
17. Krissak R, Henzler T, Reichert M, et al. Enhanced visualization of lung vessels for diagnosis of pulmonary embolism using dual energy CT angiography. *Invest Radiol.* In press.
18. Chae E, Seo J, Lee J, et al. Xenon ventilation imaging using dual energy CT in asthmatics: initial experience. *Invest Radiol.* In press.
19. Morhard D, Fink C, Graser A, et al. Cervical and cranial computed tomographic angiography with automated bone removal: dual energy computed tomography versus standard computed tomography. *Invest Radiol*. 2009;44: 293–297.
20. Sommer WH, Johnson TR, Becker CR, et al. The value of dual-energy bone removal in maximum intensity projections of lower extremity computed tomography angiography. *Invest Radiol*. 2009;44:285–292.
21. Lell MM, Kramer M, Klotz E, et al. Carotid computed tomography angiography with automated bone suppression: a comparative study between dual energy and bone subtraction techniques. *Invest Radiol*. 2009;44:322–328.
22. Graser A, Johnson TR, Hecht EM, et al. Dual-energy CT in patients suspected of having renal masses: can virtual nonenhanced images replace true nonenhanced images? *Radiology*. 2009;252:433–440.
23. Primak AN, Ramirez Giraldo JC, Liu X, et al. Improved dual-energy material discrimination for dual-source CT by means of additional spectral filtration. *Med Phys*. 2009;36:1359–1369.
24. The 2007 Recommendations of the International Commission on Radiological Protection. ICRP publication 103. *Ann ICRP.* 2007;37:1–332.
25. Holmes DR III, Fletcher JG, Apel A, et al. Evaluation of non-linear blending in dual-energy computed tomography. *Eur J Radiol*. 2008;68:409–413.
26. Huda W, Ogden KM, Khorasani MR. Converting dose-length product to effective dose at CT. *Radiology*. 2008;248:995–1003.
27. Irie T, Inoue H. Individual modulation of the tube current-seconds to achieve similar levels of image noise in contrast-enhanced abdominal CT. *Am J Roentgenol*. 2005;184:1514–1518.
28. Thieme SF, Johnson TR, Lee C, et al. Dual-energy CT for the assessment of contrast material distribution in the pulmonary parenchyma. *Am J Roentgenol*. 2009;193:144–149.
29. Pontana F, Faivre JB, Remy-Jardin M, et al. Lung perfusion with dual-energy multidetector-row CT (MDCT): feasibility for the evaluation of acute pulmonary embolism in 117 consecutive patients. *Acad Radiol*. 2008;15:1494–1504.
30. Zhang Y, Zhang ZH, Jin ZY, et al. [Radiological features of dual-energy CT lung perfusion imaging in patients with acute pulmonary embolism: comparison with CT pulmonary angiography]. *Zhongguo Yi Xue Ke Xue Yuan Xue Bao*. 2009;31:166–170.
31. Stolzmann P, Kozomara M, Chuck N, et al. In vivo identification of uric acid stones with dual-energy CT: diagnostic performance evaluation in patients. *Abdom Imaging.* In press.
32. Brenner DJ, Hall EJ. Computed tomography—an increasing source of radiation exposure. *N Engl J Med*. 2007;357:2277–2284.
33. Brink JA. Technical aspects of helical (spiral) CT. *Radiol Clin North Am*. 1995;33:825–841.
34. Ho LM, Yoshizumi TT, Hurwitz LM, et al. Dual energy versus single energy MDCT: measurement of radiation dose using adult abdominal imaging protocols. *Acad Radiol*. 2009;16:1400–1407.

Saving Dose in Triple-Rule-Out Computed Tomography Examination Using a High-Pitch Dual Spiral Technique

Wieland H. Sommer, MD, Jan C. Schenzle,* Christoph R. Becker, MD,* Konstantin Nikolaou, MD,* Anno Graser, MD,* Gisela Michalski,† Klement Neumaier,† Maximilian F. Reiser, MD,* and Thorsten R. C. Johnson, MD**

Objective: High radiation doses remain a drawback of current triple-rule-out computed tomography (CT) protocols. With dual source CT, a new high-pitch dual spiral technique offers the possibility to acquire an Electrocardiography (ECG)-gated-synchronized dataset of the whole chest in less than 1 second. The aim of this study was to compare the dose of such a protocol to a standard, nongated chest scan and to a conventional, retrospectively ECG-gated triple-rule-out protocol. Also, the efficacy and dose of this dual spiral protocol was to be compared in patients examined with this high-pitch technique and matched controls scanned with the conventional technique.

Materials and Methods: An anthropomorphic Alderson Rando phantom was equipped with thermoluminescent detectors and scanned with the high-pitch protocol (Siemens Somatom Definition Flash; 2 × 120 kVp, 426 mAs_{eff}, 128 × 0.6 mm collimation, pitch 3.2), the nongated chest scan (same scanner; 120 kVp, 160 mAs_{eff}, 128 × 0.6 mm, pitch 1.2; equivalent Computed Tomography Dose Index (CTDI) of 7.12 mGy), and the conventional gating technique (Siemens Somatom Definition; 120 kVp, 560 mAs_{eff} with ECG pulsing interval at 30%–70% of the R-R cycle, 64 × 0.6 mm, pitch 0.3). Noise was measured in air, central and peripheral soft tissue of the phantom. Conversion factors were determined based on the measured dose and the dose-length products of the scanner. The protocol was then applied with ethics committee approval in 31 patients suffering from acute chest pain. The 120 mL of contrast material (Ultravist 370, Bayer Schering Pharma) was applied at 5 mL/s. Dose was calculated based on the dose-length products and the conversion factor. Image quality was assessed by 2 readers for aorta, pulmonary arteries, and coronary arteries. The results were compared with matched controls scanned with the conventional ECG gating technique and non-ECG gated thorax scans.

Results: The dose determined with thermoluminescent dosimeters measurements amounted to 2.65, 2.68, and 19.27 mSv, respectively, for the dual spiral technique, the standard chest scan, and the conventional retrospective technique. There was no significant difference in image noise. Respective conversion factors were 0.0186, 0.0188, and 0.0180 mSv/mGy × cm. In the patient examinations, dose was 4.08 ± 0.81 mSv with the high-pitch protocol compared with 20.4 ± 5.3 mSv in the matched controls with the conventional technique, and 4.40 ± 0.83 mSv for the non-ECG gated thorax scan. Scan times were 0.7 ± 0.1 seconds for the high-pitch scan and 15 ± 3 seconds for the conventional chest pain scan. Aorta and pulmonary arteries were depicted in diagnostic quality in both groups. About 84.7% of coronary artery segments were rated as diagnostic in the high-pitch exams (95.4% below 65 bpm and only 72.8% in higher heart rates), whereas 92.9% were diagnostic with the conventional approach.

Conclusion: The high-pitch dual spiral technique requires only about one-fifth of the dose of conventional ECG gated triple-rule-out protocols, thus matching that of a standard nongated chest scan. With less than 1 second, the scan time is very short. This protocol can be recommended for patients with unclear chest pain with rhythmic heart rates below 65 bpm.

Key Words: chest pain, dual source CT, Alderson phantom, high-pitch protocol, coronary artery disease

(*Invest Radiol* 2010;45: 000–000)

There are various causes for chest pain, including pulmonary embolism, coronary artery disease, aortic dissection or aneurysm, and other nonvascular entities. Chest pain is one of the most common reasons for patient referral to the emergency department, and is responsible for 7% of emergency department visits.[1]

Multidetector row computed tomography offers a new approach to the diagnosis of thoracic pain. This approach, often referred to as "triple-rule-out," is based on an opacification of pulmonary arteries, coronary arteries, and the aorta at the same time, and can therefore be used to assess pulmonary embolism, acute coronary syndrome, and aortic dissection in 1 single examination.[2–4] Nonvascular causes of chest pain such as pneumonia and pericarditis are also covered by this examination. Several studies have proven the usefulness and cost efficacy of this triple-rule-out protocol,[5–8] and it has meanwhile become an increasingly used imaging technique for patients with acute chest pain.[9–11]

One major concern of triple-rule-out protocols remains radiation dose. Although many existing techniques, like ECG-gated tube current modulation, aim to reduce the radiation exposure of the patient, effective doses for an ECG-gated scan of the entire thorax typically range between 15 and 17 mSv,[2,9,12] but may also exceed these values in obese patients or higher heart rates.[2] Dose measurements with an Alderson Rando phantom even showed effective doses up to 32.6 mSv, depending on gender, heart rate, and ECG-pulsing.[13] There is increasing concern about the long-term risk of radiation exposure because of recent studies showing that the lifetime attributable risk of cancer associated with radiation exposure from cardiac CT studies is non-negligible.[14]

Conventional triple-rule-out protocols require a lower pitch ranging from 0.2 to 0.4 to collect sufficient data for ECG-gated image reconstruction. This causes oversampling of the scan range by imaging of the same region in several consecutive rotations (Fig. 1A). Higher pitch values could reduce the amount of oversampling significantly, however, this could lead to gaps in image acquisitions, which would be the counterpart, an undersampling of data (Fig. 1B). Recent technical advances in dual-source CT scanners include high-pitch dual spiral protocols, which are based on a simultaneous data acquisition using both tubes and detectors of the scanner, with both spiral paths turning around each other like a DNA double

Received July 28, 2009; accepted for publication (after revision) September 14, 2009.

From the Departments of *Clinical Radiology and †Radiotherapy and Radiooncology, University Hospitals-Grosshadern, Ludwig-Maximilians University, Munich, Germany.

The authors W.H.S. and J.C.S. contributed equally to this study and the manuscript.

None of the authors have financial or other kinds of interests that might pose a conflict of interest in connection with the submitted article.

Reprints: Wieland H. Sommer, MD, Department of Clinical Radiology, University of Munich, Grosshadern Campus, Marchioninistr 15, 81377 Munich, Germany. E-mail: wieland.sommer@med.uni-muenchen.de.

ISSN: 0020-9996/10/4502-0001

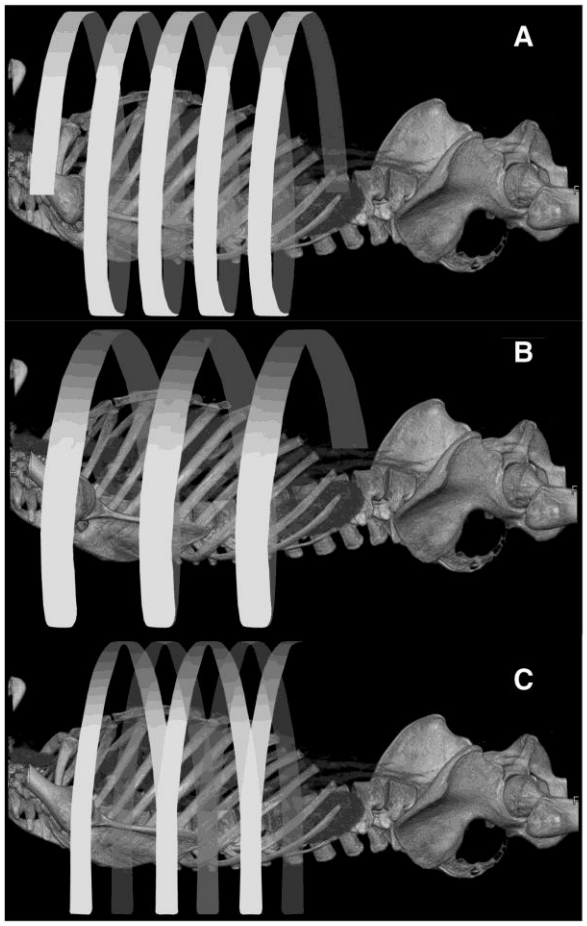

FIGURE 1. A, Standard single source chest scan, leading to an oversampling of data and therefore higher radiation doses. B, Increased pitch factors lead to an undersampling and therefore gaps in the acquired data set. C, New generation dual source scanners can use both tubes and detectors simultaneously with very high pitch factors to acquire a dual spiral scan with both spiral acquisitions complementing each other.

helix.[15,16] Thus, an extremely fast, nonoverlapping but continuous volume coverage can be achieved. Pitch values range up to 3.4, leading to an acquisition of the whole thorax in 0.6 mm isotropic resolution within less than 1 second (Fig. 1C). As the second generation dual source CT scanner (Siemens Definition Flash) acquires 128 slices simultaneously, this high-pitch results in an extremely fast volume coverage of 430 mm/sec. This recently developed high-pitch, subsecond protocol might make it possible to identify the cause of acute chest pain, and may lower radiation dose to a fraction of that of current protocols.

The aim of the current study was to objectively measure dose and assess image quality of such a high-pitch triple-rule-out protocol and to compare it to our previously used conventional "triple-rule-out" protocol. Also, the dose was to be compared with a standard chest scan acquired at 120 kVp for reference. For these 3 different scans, effective radiation dose and image noise were assessed in an anthropomorphic Alderson-Rando phantom using thermoluminescent dosimeters. Furthermore, the high-pitch triple-rule-out protocol was to be tested for its clinical applicability in a group of patients and compared with a patient cohort scanned with a conventional triple-rule-out protocol.

MATERIALS AND METHODS

The comparison of high-pitch chest scan and conventional triple-rule-out protocols was performed in 2 different ways. The aim of part A was to determine representative radiation doses, image noise, and effective radiation dose (E)/dose-length products (DLP) conversion factors both for the new high-pitch acquisition and for the conventional ECG-gated triple-rule-out protocol using an Alderson-Rando phantom. Furthermore, the high-pitch triple-rule-out protocol was compared with a standard non-ECG-gated chest protocol. Part B investigates the clinical feasibility of the high-pitch protocol in a group of patients. Image quality parameters of this group of patients were compared with a matched group of patients who had been examined with the conventional triple-rule-out protocol.

Part A: Alderson-Rando Phantom Study

Scan Protocols

To determine representative radiation doses, image noise and E/DLP conversion factors, different protocols were applied on an anthromorphic Alderson-Rando phantom (Alderson Research Laboratories Inc., Stanford, CT).

1. Standard non-ECG synchronized chest scan.
2. High-pitch dual spiral triple-rule-out protocol.
3. Conventional, retrospectively ECG-gated triple-rule-out protocol.[2,3]

Scans 1 and 2 were performed on the new generation dual source CT-scanner (Somatom Definition Flash; Siemens Healthcare, Forchheim, Germany), whereas scan 3 was performed using the previous dual source CT-scanner (Somatom Definition; Siemens Healthcare, Forchheim, Germany).

1. The standard non-ECG synchronized chest scan was performed using the following parameters:120 kVp tube voltage; 160 mAs_{eff} current time product with dose modulation (CareDose 4D); 128 × 0.6 mm collimation at a pitch of 1.2; 276 mm scan length; 7.11 mGy CT Dose Index; rotation time, 500 milliseconds.
2. To determine comparable image noise for the high-pitch ECG-synchronized triple-rule-out protocol, a row of scans was performed in which only the tube current was modified, whereas all remaining parameters were kept unchanged: 2 × 120 kVp tube voltage, tube current with dose modulation (CareDose 4D) was steadily increased from 320 mAs_{eff} to 430 mAs_{eff} in steps of 10 mAs (ie, 320 mAs_{eff}, 330 mAs_{eff}, 340 mAs_{eff}, . . . 430 mAs_{eff}). A further scan was performed with 426 mAs_{eff}, because this current resulted in approximately the same CTDI (7.12 mGy) and image noise as our standard chest protocol (see results). Scan length was 276 mm, pitch 3.2, collimation 128 × 0.6 mm, rotation time 280 milliseconds. This row was performed without thermoluminescent dosimeters (TLD) as an initial approach to obtain a comparable signal-to-noise ratio as scan 1. Regarding the temporal resolution of this acquisition, it is important that the 2 tubes and detectors are angulated at 94 degree in this dual source scanner. Since 180 degree of projection data are required for reconstruction of cross-sectional images, the projection data set are completed if the gantry has rotated 94 degree. Because the rotation time of this new dual source CT-Scanner is 280 milliseconds, this results in an image acquisition time of 94/360 × 280 milliseconds = 73 milliseconds.

3. The phantom was examined using the conventional triple-rule-out protocol on the Siemens Definition Dual Source CT-scanner with the following parameters: scan length 276 mm, tube voltage 120 kVp, tube current time product with dose modulation (CareDose 4D) 560 mAs_{eff}, pitch 0.3, collimation 64 × 0.6 mm, rotation time 330 milliseconds, wide pulsing window of 30% to 70% of the R-R_cycle on a simulated heart rate of 70 bpm with a CTDI of 37.2 mGy. As the 2 tubes and detectors are mounted orthogonally at 90 degree in this scanner, the temporal resolution can be calculated as a quarter of the rotation time, ie, 83 milliseconds.

Noise Measurements

A region of interest (ROI) analysis was performed to determine and compare noise in the center of the phantom, in the periphery of the phantom and in the air outside the phantom. The soft tissue of the mediastinum was chosen for the central measurements, the soft tissue of the thoracic wall served for peripheral measurements. All measurements were performed for 5 different z-axis positions of the phantom with a standardized ROI size of 3 cm^2. Image noise was defined as the standard deviation (SD) of HU values of the ROI, placed in a homogenous region.

Radiation Dose

For objective dose measurements of the 3 protocols, an anthropomorphic Alderson-Rando phantom was used,[13,17–20] and equipped with 58 TLDs with dimensions of 1 × 1 × 6 mm (TLD-100H, Bicron-Harshow, Radiation Measurement Products, Cleveland, OH). The phantom was placed in a standardized central position in the gantry and the above-mentioned different examination protocols were performed. Each of the 3 protocols was repeated 10 times to even out statistical variations and to obtain a higher total exposure, because TLDs are designed for radiotherapy and therefore measurements are more precise in higher effective doses. Organ doses were assessed for 58 different positions in the Alderson-Rando phantom, depending on the anatomic position of each organ. For large organs, a TLD was placed in each slice that contained a section of the organ to account for z-axis dose variability. The following numbers of TLDs were allocated to the different organs: lung (n = 14), thyroid gland (n = 1), esophagus (n = 4), spine (n = 5), mediastinum (n = 4), liver (n = 6), stomach/colon (n = 2), and skin (n = 22). Irradiated TLDs were evaluated within 24 hours after exposure using a TLD reader (TL Picoprocessor 2080 and TL Detector 2000D). The equivalent dose was calculated by multiplying the organ dose with the tissue weighting factor according to ICRP-60[21,22] and summing the organ doses.

E/DLP Conversion Factors for the CT Scan Protocols

To obtain representative E/DLP conversion factors for the 3 protocols mentioned above, the effective radiation dose (E) from the TLD-measurements and DLP from the patient protocol were recorded. The E/DLP conversion factor (k) was calculated as the ratio of equivalent dose in mSv and DLP in mGy × cm.[23,24]

Part B: Clinical Application of the High-Pitch and the Conventional Triple-Rule-Out Protocol

Patient Examinations With Non-ECG Gated Thorax Scans

Of all patients who were examined with a non-ECG gated thorax scan in daily clinical routine, 30 patients were matched by the BMI to patients who received the high-pitch chest pain protocol. For non-ECG gated thorax scans, the same parameters and the same scanner (Siemens Definition Flash) as in the phantom measurement were used. Tube current modulation was also applied (CareDose4D). This cohort of patients served to compare the effective doses between non-ECG gated chest scans and high-pitch chest pain protocols not only in the phantom but also in patients.

The DLP was taken from the patient protocol; effective doses were calculated using the conversion weighting factor determined in our Alderson-Rando phantom study (part A).

Patient Examinations With High-Pitch Dual Spiral Protocol

The high-pitch protocol was applied in 31 patients (15 male, 16 female; mean age, 65.2 ± 14.3 years; range: 32–86 years; weight, 74 ± 9 kg; cf; Table 1) to identify the cause of chest pain. Written informed consent was obtained from each patient. The study was approved by the local ethics committee. Only patients with sinus rhythm were included in the study. Exclusion criteria were known allergy to iodinated contrast material and age below 30 years, both of which did not occur in otherwise eligible patients.

For patient examinations, we used the same scan parameters as in the phantom measurements: 128 × 0.6 mm slice collimation with z-flying focal spot, 426 mAs_{eff} tube current time product with attenuation based modulation (CareDose4D), 120 kVp tube voltage, 430 mm/s table speed at a pitch of 3.2. As contrast material we applied 120 mL of iodinated contrast material (Ultravist 370; Bayer Schering Pharma) at a flow rate of 5 mL/s followed by a saline chaser bolus (100 mL at 5 mL/s). For timing, a test bolus of 15 mL contrast agent was injected. After a delay of 10 seconds, 20 subsequent axial images were obtained at the level of the ascending aorta at an interval of 1 second. The time of maximum enhancement within a ROI in the ascending aorta was determined in seconds after injection start, and the resulting time interval was chosen as scan delay. Bolus tracking may be regarded as preferable to save contrast material and eliminate variability because of different breathing. Meanwhile this option is available, but at the time of our study it had not been implemented by the CT manufacturer for this scan mode. The scan range encompassed the entire chest from the lung apex to the diaphragm. ECG synchronization was used to verify that the range that will be motion-free during a late diastolic phase covered the entire heart. Data acquisition of the heart commenced at 55% of the RR cycle, and the scans were performed in craniocaudal direction. Because the diastolic phase shortens in higher heart rates systolic contraction may already commence when the end of the spiral scan is still being acquired, and for this reason the craniocaudal scan direction was chosen to ensure that at least the proximal parts of the coronary arteries are depicted without motion artifacts. The continuous spiral acquisition implies an increasing delay after the R-peak, so that the last images of the scan range are acquired about 180 to 240 milliseconds

TABLE 1. Comparison of the Patients Who Underwent the High-Pitch Dual Spiral Chest Pain Protocol and the Controls Who Were Previously Scanned With a Conventional Chest Pain Protocol, Using Retrospective Gating Technique

	Patients	Controls	*P*
Age (yr)	65 ± 14	63 ± 15	0.72
Weight (kg)	73 ± 13	74 ± 13	0.67
Heart rate (bpm)	66 ± 17	69 ± 15	0.71
Scan time (sec)	0.7 ± 0.1	15 ± 3	<0.0001
Non-diagnostic exams	4	1	0.12
Non-diagnostic coronary segments	15%	7%	0.11
Dose (mSv)	4.1 ± 0.8	20.4 ± 5.3	<0.0001

later than the first images. For data reconstruction, axial images were reconstructed with a slice thickness of 0.6 mm and 0.5 mm increment using a standard B26f soft tissue kernel.

Image quality was determined for each patient on a 4-point scale (1 = very good image quality; 2 = good image quality with restrictions because of image noise; 3 = limited image quality because of image noise or motion artifacts, but still diagnostic for chest pain assessment; 4 = nondiagnostic image quality). The pulmonary arteries, the aorta, and the coronary arteries were rated on as 1 = diagnostic and 2 = nondiagnostic visualization of the segment/vessel. This was performed separately for the pulmonary arteries, the aorta, and all of 15 possible coronary segments, according to the American Heart Association reporting system, depending on the individual anatomy. Image quality was rated as nondiagnostic if either the aorta, the pulmonary arteries or the left anterior descendent (LAD), the circumflex artery (RCX), or the right coronary artery (RCA) (coronary artery segments 1, 2, 3, 5, 6, 7, or 11) could not be assessed adequately.[25,26] All ratings were performed by 2 experienced radiologists. In case of diverging ratings, a consensus was found between the 2 readers.

In all examinations, CT numbers ±SDs were measured in the pulmonary trunk, the aorta, and the proximal and the distal left and right coronary arteries.

From the DLP of the patient protocol, effective doses were calculated using the organ-specific weighting factor for the chest which we had determined in our Alderson-Rando phantom study (part A).

Patient Examinations With the Conventional Chest Pain Protocol

Of a previous cohort of patients who had presented with chest pain symptoms in the emergency department and therefore had been examined with our previous conventional, retrospectively ECG-gated triple-rule-out protocol, 31 patients were chosen for comparison of radiation exposure and image quality. Those patients were matched according to heart rate, gender, and body weight. Furthermore, only patients with sinus rhythm were chosen as matches from the cohort. All of them had been examined on a dual source CT system (Somatom Definition Dual Source, Siemens Healthcare, Forchheim, Germany). Scan parameters were 0.33 seconds gantry rotation time, 120 kVp tube voltage, 560 mAs_{eff} effective tube current time product with online dose modulation, and 0.6 mm collimation. A body-weight adapted contrast material injection protocol was used; the mean contrast volume was 130 mL at a flow of 4.3 mL/s (Ultravist 370, Bayer Schering Pharma). Pitch and tube current modulation were adapted automatically to the heart rate of the patient.[2,27] Pitch values ranged from 0.2 to 0.48, whereas the full tube current was only applied at 70% of the cardiac cycle for heart rates below 70 bpm and between 30% and 70% for higher heart rates. This wide pulsing window served to render a systolic reconstruction possible in higher heart rates. DLP values were recorded from the patient protocols, and effective radiation doses were calculated using the E/DLP conversion factors, which we had determined in our Alderson-Rando phantom study.

Image quality was determined for each patient on the same 4-point scale as mentioned above. As in the high-pitch triple-rule-out patient group, the pulmonary arteries, the aorta, and the coronary artery segments were rated as 1 = diagnostic or 2 = nondiagnostic visualization of the segment/vessel.

Statistical Analysis

Continuous variables are given as mean ±SD. To compare continuous variables of the patients and their matched controls scanned, the Mann-Whitney *U* test was applied. Nominal data were compared using the χ^2 test. *P* values below 0.05 were considered significant. A Spearman rank correlation analysis was performed for heart rate and image quality.

RESULTS

Part A: Alderson-Rando Phantom Study

Noise Measurements

The phantom examinations performed for the noise measurements of the high-pitch protocol at an effective tube current-time product of 426 mAs_{eff} showed an identical CTDI as our standard chest protocol, ie, 7.12 mGy. In the center of the phantom, the noise of the 120 kVp standard chest scan and the high-pitch acquisition were nearly equal with 9.22 and 9.16 HU. In the periphery of the phantom, a cardiac bow-tie filter increased the noise with the high-pitch acquisition by about 11.8% over the standard 120 kVp scan, but with 8.74 HU it still remained slightly below the noise in the center. Because all anatomic structures, which may be responsible for vascular causes of chest pain are located centrally in the thorax, this tube current (426 mAs_{eff}) was chosen as standard setting for the patient examinations. Averaged noise values of all 15 ROIs for the standard chest protocol, the high-pitch protocol, and the conventional chest pain protocol were 8.01 ± 1.80, 8.17 ± 1.67, and 7.51 ± 1.86 HU, respectively. These values were not significantly different ($P > 0.05$; cf. Table 2).

Radiation Dose

TLD measurements of our standard chest protocol, using 120 kV tube voltage and 160 mAs_{eff}, resulted in an equivalent dose of 2.68 mSv. The corresponding DLP value from the patient protocol was 144 mGy × cm.

The high-pitch triple-rule-out protocol with the equivalent CTDI and a tube current of 426 mAs_{eff} had a measured effective equivalent dose of 2.65 mSv. Thus, it resulted in 98.8% of the dose of the standard chest protocol. The DLP in the patient protocol was 141 mGy × cm.

The conventional triple-rule-out, using the Siemens Definition Dual Source CT-scanner and a wide pulsing window at a simulated heart rate of 70 bpm and retrospective gating, resulted in a measured equivalent dose of 19.27 mSv. The corresponding DLP in the patient protocol was 1070 mGy × cm (cf. Table 2).

TABLE 2. Comparison of the Results From the Alderson-Rando Phantom Study for the Standard Non-ECG Gated Chest Scan, the High-Pitch Dual Spiral Chestpain Protocol, and the Retrospectively ECG-Gated Chest Pain Scan

	Standard Non-ECG Gated Chest Scan	High-Pitch Dual Spiral Chestpain Protocol	Retrospectively ECG-Gated Chestpain Protocol
Tube voltage (kV)	120	120	120
Tube current (mAs_{eff})	160	426	560
Collimation (mm)	128 × 0.6	128 × 0.6	64 × 0.6
Scan range (mm)	276	276	276
Image noise (HU)	8.01 ± 1.80	8.17 ± 1.67	7.51 ± 1.86
DLP (mGy × cm)	144	141	1070
Radiation dose (mSv)	2.68	2.65	19.27
E/DLP conversion factor	0.0186	0.0188	0.0180

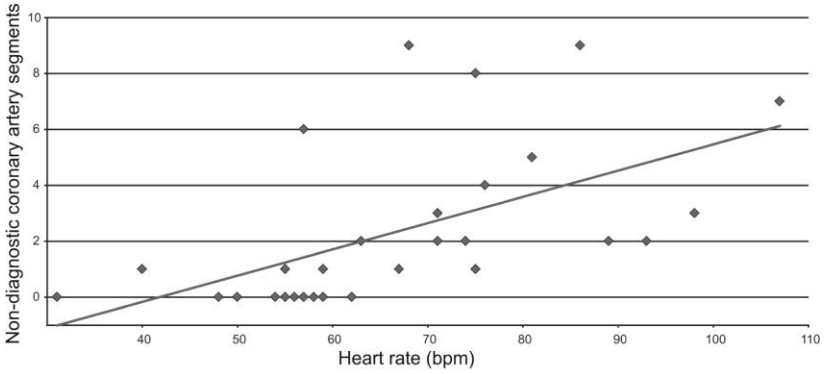

FIGURE 2. Number of nondiagnostic coronary artery segments versus heart rate in beats per minute (bpm). With higher heart rates, the number of nondiagnostic artery segments rises. This is caused by the shortening of the diastole at higher heart rates and therefore the inferior parts of the coronary artery tree already show motion artifacts.

Calculation of E/DLP Conversion Factors for the Different CT Protocols

For the standard 120 kV non-ECG gated chest scan on the Siemens Definition Flash dual source CT scanner, the E/DLP conversion factor (k) amounted to 0.0186 mSv/mGy × cm. The values of the high-pitch protocol resulted in a conversion factor k = 0.0188 mSv/mGy × cm. For the conventional triple-rule-out protocol, using the Siemens Definition Dual Source CT-scanner, the conversion factor k had a value of 0.0180 mSv/mGy × cm (cf. Table 2).

Part B: Clinical Application of the High-Pitch and the Conventional Triple-Rule-Out Protocol

Patient Examinations With Non-ECG Gated Thorax Scans

The standard thorax scan resulted in a mean DLP of 232 ± 44 mGy (range, 144–332 mGy). Using the established E/DLP conversion factor of 0.0188 from part A of the results, this corresponds to a mean effective dose of 4.40 ± 0.83 mSv (range, 2.70–6.24 mSv).

Patient Examinations With High-Pitch Dual Spiral Protocol

All patient examinations were completed without complications. Scan time ranged from 0.6 to 0.8 seconds. The combination of the test bolus and the contrast injection protocol lead to a sufficient vascular opacification in all but 1 patient. In this individual, opacification of the coronary arteries was insufficient in spite of an accurate test bolus, presumably because of congestive heart failure and a very low left ventricular ejection fraction. Mean attenuation values for the main pulmonary artery were 412 ± 116 HU, for the aorta 377 ± 103 HU. In the proximal and distal left coronary artery density was 399 ± 128 HU and 272 ± 100 HU, respectively, and in the proximal and distal right coronary artery 376 ± 103 HU and 331 ± 122 HU, respectively.

The aorta and the pulmonary artery were clearly depicted in all examinations and rated as diagnostic in all cases, regardless of the heart rate. For the coronary arteries, 382 of 451 segments were rated as diagnostic (=84.7%), whereas the remaining 69 were rated as nondiagnostic (=15.3%). Since the duration of the diastole decreases with higher heart rates, there was a high dependency of heart rate and the motion artifacts of coronary arteries. The mean heart rate of all patients was 66 ± 17 bpm. In patients with heart rates below 65 bpm (N = 16), 95.4% (226 of 237) coronary artery segments were depicted in diagnostic quality, whereas only 72.8% (155 of 213) of coronary artery segments were rated as diagnostic in patients with heart rates above 65 bpm ($P < 0.0001$; Fig. 2). For the patient-based evaluation, the dataset was rated as diagnostic if the main coronary arteries, ie, segments 1, 2, 3, 5, 6, 7, and 11 were well opacified and did not show motion artifacts. Using these criteria, the coronary artery datasets of 4 of 31 patients had to be rated as nondiagnostic, all of them with heart rates over 65 bpm.

Of the 31 patients undergoing the high-pitch examination for acute chest pain, 11 had no radiologic correlate of these symptoms (see Fig. 3 as an example), 7 showed acute pulmonary embolism (Fig. 4), and 13 patients had coronary artery disease (Fig. 5); there were no aortic dissections or acute aneurysms.

Image quality was rated as 1 (=very good image quality) in 14 cases, as 2 (=good image quality with restrictions because of image noise) in 10 cases, as 3 (=mediocre image quality because of image noise or motion artifacts, but still diagnostic for chest pain assessment) in 3 cases, and as 4 (=nondiagnostic image quality) in 4 cases. These 4 nondiagnostic cases were caused by motion artifacts of the coronary arteries, especially in the caudal scan range, and correspond to the 4 cases of nondiagnostic coronary arteries. This was also dependent on the heart rate: mean image quality was 1.38 ± 0.72 below 65 bpm, and 2.47 ± 0.92 above 65 bpm ($P < 0.05$). A rank-correlation analysis between heart rate and image quality showed a Spearman ρ of 0.709 ($P = 0.0001$).

The high-pitch protocol resulted in a mean DLP of 217 ± 43 mGy (range, 127–281 mGy). Using the established E/DLP conversion factor of 0.0188 from part A of the results, this corresponds to a mean effective dose of 4.08 ± 0.81 mSv (range, 2.39–5.28 mSv).

Patient Examinations With the Conventional Chest Pain Protocol

The gender distribution (15 male, 16 female), age (63 ± 14 years), weight (73 ± 10 kg), and heart rates (69 ± 8 bpm) did not differ significantly between the patients and their matched controls (cf. Table 1). Scan duration with the conventional ECG gated protocol had been 15 ± 3 seconds. The depiction of aorta and pulmonary artery were rated as diagnostic in all cases. The mean heart rate was 69 ± 15 bpm; 421 of 453 coronary artery segments were rated as diagnostic (=92.9%), whereas the remaining 32 were rated as nondiagnostic. There was no clear relation between heart rate and motion artifacts in the coronary arteries. Regarding a patient-based assessment, the nondiagnostic ratings only occurred in side branches, ie, the main coronary arteries were rated as diagnostic in all 31 matched control patients.

Among the diagnoses in the matched control patients there were 8 negative exams, 6 had an acute pulmonary embolism and 13 patients had been diagnosed with significant coronary artery disease. There had been one case of an acute aortic dissection. Three patients

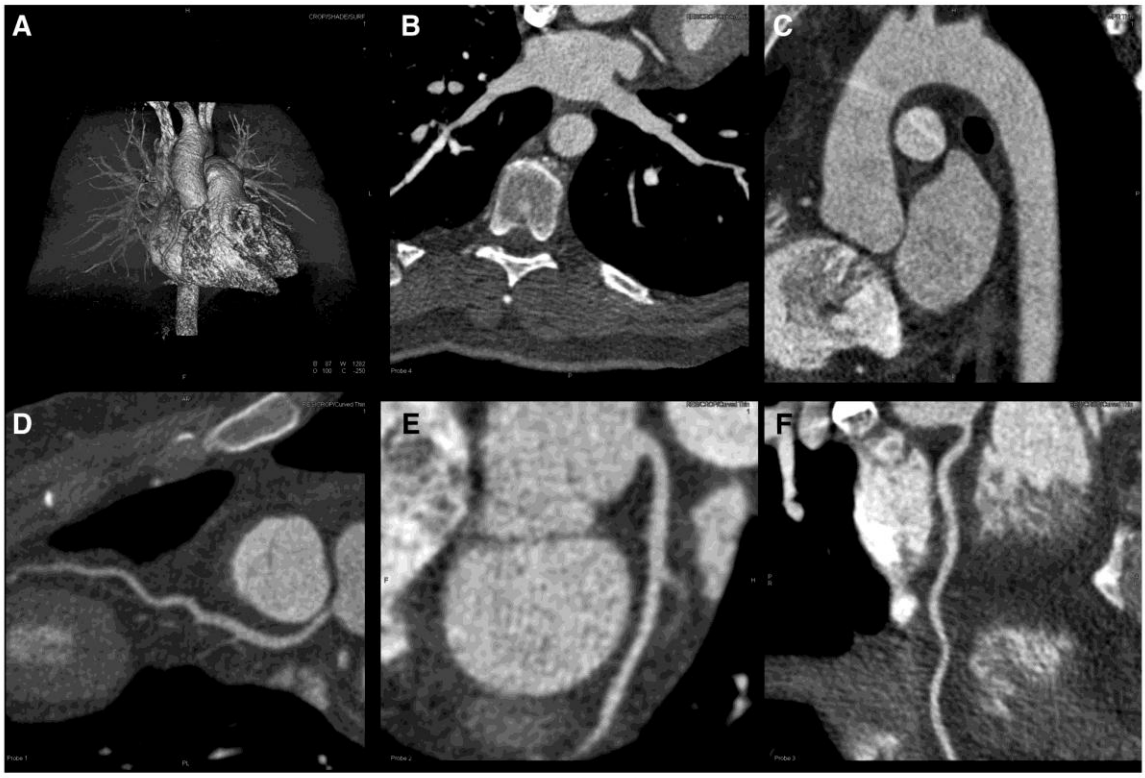

FIGURE 3. VRT reconstruction of the chest (A), curved MPR of the pulmonary arteries (B), MPR of the aorta (C), curved MPRs of the LAD (D), RCX (E) and RCA (F) in a 61-year-old male patient who was examined using the high pitch dual spiral triple-rule-out protocol because of unclear chest pain. No morphologic correlate of the chest pain could be found. The heart rate in this patient was 62 bpm.

had nonvascular causes of chest pain, ie, pneumonia, pneumothorax, and pulmonary metastases.

Image quality was rated as 1 (=very good image quality) in 14 cases, as 2 (=good image quality with restrictions because of image noise) in 12 cases, as 3 (=mediocre image quality because of image noise or motion artifacts, but still diagnostic for chest pain assessment) in 4 cases, and as 4 (=nondiagnostic image quality) in 1 case with insufficient contrast opacification. A rank-correlation analysis between image quality rating and hart rate showed a Spearman ρ of 0.142 ($P = 0.44$).

Mean DLP values were 1135 mGy, with a range from 818 to 1575 mGy. Using a conversion factor of 0.0180 as established in the Alderson-Rando phantom study for this scanner (part A), this corresponds to a mean effective dose of 20.4 ± 5.3 mSv (range, 14.7–28.4 mSv) (cf. Table 1). Comparing the mean effective doses of the new high-pitch protocol and the standard chest pain protocol, the former only uses 19.9% of the dose of the latter.

DISCUSSION

CT examination protocols for chest pain assessment have been shown to be effective for the diagnosis of different causes of vascular and nonvascular pathologies.[9] With technical advances in recent years, the visualization of coronary arteries has continuously improved, especially with the introduction of dual source CT scanners,[2,16,28–31] which doubled the previous temporal resolution. Also, the first dual source CT scanner (Siemens Definition Dual Source) lead to technical innovations in dual energy imaging, which meanwhile resulted in several clinical applications.[32–34] Other technical innovations for chest pain protocols include multidetector row computed tomography scanners with up to 320 rows, which are helpful for a fast acquisition of larger volumes. Initial results lead to high-image quality, however, radiation exposure of these protocols still ranges between 7 and 14 mSv, and the range of an ECG-triggered acquisition is limited to the detector width, which would not cover the entire chest.[35] A recently introduced new dual source CT system has the potential to greatly reduce radiation exposure in thoracic scans. Rather high radiation doses in earlier chest pain protocols limited their wide-spread use. Specific protocols for aortic dissection or pulmonary embolism involved lower radiation doses, and were therefore preferred in patients with complaints suggestive of a specific cause. Generally, the dose delivered by an ECG-gated conventional chest pain protocol with its low pitch and data oversampling are 4 to 5 times higher than the radiation dose of a non-ECG gated pulmonary embolism protocol.

The novel high-pitch dual spiral protocol has the potential to revolutionize triple-rule-out protocols, because its radiation dose is only a fraction of former chest pain protocols, thus matching the dose of a nongated standard chest scan. Our phantom measurements confirmed a dose saving of 86.5%. Using the E/DLP conversion factors determined in the technical part of this study, this difference translates into about 80% in the comparison of the matched patient cohorts examined with the new high-pitch dual-spiral protocol and

FIGURE 4. Seventy-five-year-old male patient with acute chest pain examined with the high-pitch technique. There is a pulmonary embolism in the left upper lobe pulmonary artery. Additionally, there are extensive pleural effusions on both sides. The heart rate in this patient was 74 bpm.

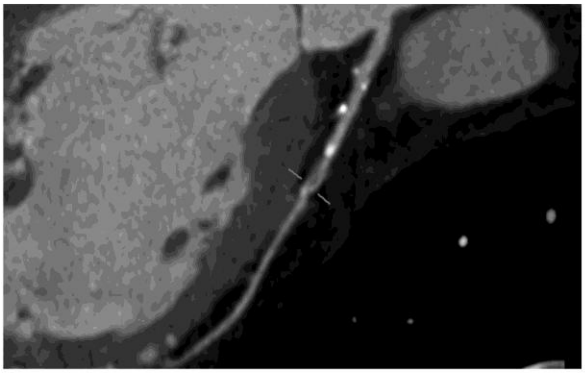

FIGURE 5. Curved MPR of the left circumflex coronary artery in a 59-year-old patient who presented with unclear chest pain. There is a soft plaque in the proximal coronary artery which leads to a stenosis of approximately 70% of the arterial lumen. The heart rate in this patient was 63 bpm.

the conventional, ECG gated method. The high-pitch chest pain protocol resulted in an effective dose of 2.65 mSv in the phantom study and in 4.1 mSv in the patient study. This difference can be attributed to the rather slim Alderson-Rando phantom compared with the standard patient. Furthermore, a shorter scan range in the phantom study may have contributed to this difference.

There is a considerable variability in tube current values between the different protocols, both in phantom and patient examinations, although the tube current was adjusted to achieve similar image noise for all 3 protocols. The differences in tube current time product settings can be attributed to differences in rotation time, pitch, prefiltration, and scanner geometry. Therefore, the tube current values are not directly proportional to image noise or radiation exposure, and only CTDI values should be regarded as a measure for dose.

Previous "Triple-rule-out" protocols also required breath hold times of at least 15 seconds,[2] which represents a significant limitation, especially in patients with severe dyspnea. The new high-pitch dual spiral protocol requires an extremely short breath-hold of less than 1 second. The high-pitch and the conventional triple-rule-out protocol used about the amount of contrast material in our current study, considering that a test bolus was necessary for the high-pitch protocol. The high-pitch protocol resulted in an excellent opacification of the aorta, the pulmonary arteries, and the coronary arteries. Because of the short-scan-time, it might be possible to use a short and dense bolus and reduce the amount of contrast material. However, further studies are require to specifically investigate this issue.

Unlike conventional triple-rule-out protocols, high-pitch protocols commence acquiring projection data of the heart at a certain percentage of the heart cycle, typically between 50% and 60%, and then record subsequent image data in z-direction at subsequent timepoints of the heart cycle. Therefore, only one nonoverlapping acquisition of the data set are recorded, and no pulsing window is used as in conventional chest pain protocols. For motion-free depiction of the coronary arteries, the acquisition of the entire heart has to be completed within 1 diastolic phase of the cardiac cycle. Because the duration of the diastole is highly dependent on the heart rate, it is comprehensible that the motion-free depiction is limited to the cranial part of the coronary arteries if diastole becomes too short in high heart rates. Given a table speed of 430 mm/s with this technique, a 10 cm scan range covering the heart is acquired within about 230 milliseconds, and motion artifacts occur in the inferior part of the coronary artery tree if the duration of the diastolic resting phase is shorter.

For the ECG synchronization, the last 3 R-R cycles before image acquisition are taken into account to predict the optimal time point for the acquisition of the scan range covering the hart, usually between 50% and 60% of the cardiac cycle. The first image of the heart is recorded at this time point, whereas subsequent images are acquired at later phases of the cardiac cycle. Therefore, it has to be emphasized that the heart is not entirely imaged at the same time point, as in standard prospective triggering coronary CT-angiography, but rather at a slightly increasing delay in the cardiac cycle. This may also have lead to the higher number of nondiagnostic examinations in the high-pitch protocol ($n = 4$), compared with the conventional chest pain protocol ($n = 1$). Although not statistically significant, this trend suggests that dual spiral acquisition is more vulnerable at high heart rates. Although the nominal resolution in the image is the same, the increasing delay after the R-peak makes the overall acquisition time for the scan range of the heart quite wide with about 200 milliseconds. In low heart rates, this is sufficient, because the diastolic resting window is quite long. This window diminishes in higher heart rates, and therefore it becomes impossible to acquire the entire heart without motion artifacts during 1 diastolic phase. For a detailed quantitative analysis of this issue, further studies have to be performed with larger numbers of patients.

However, the dependency of the image quality on the heart rate is the only major drawback of the high-pitch dual spiral protocol, whereas the fast scan speed and the low dose represent significant advantages. Therefore, it seems adequate to use beta-blockers in chest pain patients with higher heart rates to render a high-pitch dual spiral examination feasible.

CONCLUSION

The high-pitch dual spiral acquisition mode of a new dual source CT system requires only about one-fifth of the dose of former

protocols. The radiation exposure is very similar to a standard non-ECG gated chest scan. This protocol can be recommended for patients with unclear chest pain presenting with rhythmic heart rates below 65 bpm. In patients with higher heart rates, application of beta blockers or the conventional ECG gated protocol should be considered to reliably achieve a sufficient image quality.

ACKNOWLEDGMENTS

This study was supported with an unrestricted grant by Bayer Schering Pharma AG. The authors thank Jarah Al-Tubaikh for help with preparation of the figures, and Veronika Eberle for constructive comments on the manuscript.

REFERENCES

1. American College of Emergency Physicians. Clinical policy for the initial approach to adults presenting with a chief complaint of chest pain, with no history of trauma. *Ann Emerg Med*. 1995;25:274–299.
2. Johnson TR, Nikolaou K, Becker A, et al. Dual-source CT for chest pain assessment. *Eur Radiol*. 2008;18:773–780.
3. Johnson TR, Nikolaou K, Wintersperger BJ, et al. ECG-gated 64-MDCT angiography in the differential diagnosis of acute chest pain. *Am J Roentgenol*. 2007;188:76–82.
4. Takakuwa KM, Halpern EJ. Evaluation of a "triple rule-out" coronary CT angiography protocol: use of 64-Section CT in low-to-moderate risk emergency department patients suspected of having acute coronary syndrome. *Radiology*. 2008;248:438–446.
5. Hoffmann U, Nagurney JT, Moselewski F, et al. Coronary multidetector computed tomography in the assessment of patients with acute chest pain. *Circulation*. 2006;114:2251–2260.
6. Sato Y, Matsumoto N, Ichikawa M, et al. Efficacy of multislice computed tomography for the detection of acute coronary syndrome in the emergency department. *Circ J*. 2005;69:1047–1051.
7. Goldstein JA, Gallagher MJ, O'Neill WW, et al. A randomized controlled trial of multi-slice coronary computed tomography for evaluation of acute chest pain. *J Am Coll Cardiol*. 2007;49:863–871.
8. Hoffmann U, Pena AJ, Moselewski F, et al. MDCT in early triage of patients with acute chest pain. *Am J Roentgenol*. 2006;187:1240–1247.
9. Frauenfelder T, Appenzeller P, Karlo C, et al. Triple rule-out CT in the emergency department: protocols and spectrum of imaging findings. *Eur Radiol*. 2009;19:789–799.
10. Schertler T, Frauenfelder T, Stolzmann P, et al. Triple rule-out CT in patients with suspicion of acute pulmonary embolism: findings and accuracy. *Acad Radiol*. 2009;16:708–717.
11. Takakuwa KM, Halpern EJ, Gingold EL, et al. Radiation dose in a "triple rule-out" coronary CT angiography protocol of emergency department patients using 64-MDCT: the impact of ECG-based tube current modulation on age, sex, and body mass index. *Am J Roentgenol*. 2009;192:866–872.
12. Gallagher MJ, Raff GL. Use of multislice CT for the evaluation of emergency room patients with chest pain: the so-called "triple rule-out." *Catheter Cardiovasc Interv*. 2008;71:92–99.
13. Ketelsen D, Thomas C, Werner M, et al. Dual-source computed tomography: estimation of radiation exposure of ECG-gated and ECG-triggered coronary angiography. *Eur J Radiol*. In press.
14. Einstein AJ, Henzlova MJ, Rajagopalan S. Estimating risk of cancer associated with radiation exposure from 64-slice computed tomography coronary angiography. *JAMA*. 2007;298:317–323.
15. Flohr TG, Bruder H, Stierstorfer K, et al. Image reconstruction and image quality evaluation for a dual source CT scanner. *Med Phys*. 2008;35:5882–5897.
16. Petersilka M, Bruder H, Krauss B, et al. Technical principles of dual source CT. *Eur J Radiol*. 2008;68:362–368.
17. Nickoloff EL, Alderson PO. A comparative study of thoracic radiation doses from 64-slice cardiac CT. *Br J Radiol*. 2007;80:537–544.
18. Ketelsen D, Luetkhoff MH, Thomas C, et al. Estimation of the radiation exposure of a chest pain protocol with ECG-gating in dual-source computed tomography. *Eur Radiol*. 2009;19:37–41.
19. Thomas C, Patschan O, Ketelsen D, et al. Dual-energy CT for the characterization of urinary calculi: in vitro and in vivo evaluation of a low-dose scanning protocol. *Eur Radiol*. 2009;19:1553–1559.
20. Deak PD, Langner O, Lell M, et al. Effects of adaptive section collimation on patient radiation dose in multisection spiral CT. *Radiology*. 2009;252:140–147.
21. The 2007 Recommendations of the International Commission on Radiological Protection. ICRP publication 103. *Ann ICRP*. 2007;37:1–332.
22. Cho KW, Kim YM. Implementation of the ICRP 2007 recommendations in Korea. *Appl Radiat Isot*. 2009;67:1286–1289.
23. Huda W, Ogden KM, Khorasani MR. Converting dose-length product to effective dose at CT. *Radiology*. 2008;248:995–1003.
24. Huda W. Computing effective doses from dose-length product in CT. *Radiology*. 2008;248:321–322.
25. Nikolaou K, Rist C, Wintersperger BJ, et al. Clinical value of MDCT in the diagnosis of coronary artery disease in patients with a low pretest likelihood of significant disease. *Am J Roentgenol*. 2006;186:1659–1668.
26. Nikolaou K, Knez A, Rist C, et al. Accuracy of 64-MDCT in the diagnosis of ischemic heart disease. *Am J Roentgenol*. 2006;187:111–117.
27. Flohr TG, McCollough CH, Bruder H, et al. First performance evaluation of a dual-source CT (DSCT) system. *Eur Radiol*. 2006;16:256–268.
28. Rist C, Johnson TR, Becker CR, et al. New applications for noninvasive cardiac imaging: dual-source computed tomography. *Eur Radiol*. 2007;17(suppl 6):F16–F25.
29. Schertler T, Scheffel H, Frauenfelder T, et al. Dual-source computed tomography in patients with acute chest pain: feasibility and image quality. *Eur Radiol*. 2007;17:3179–3188.
30. Rist C, Johnson TR, Muller-Starck J, et al. Noninvasive coronary angiography using dual-source computed tomography in patients with atrial fibrillation. *Invest Radiol*. In press.
31. Mahnken AH, Bruners P, Schmidt B, et al. Left ventricular function can reliably be assessed from dual-source CT using ECG-gated tube current modulation. *Invest Radiol*. 2009;44:384–389.
32. Morhard D, Fink C, Becker C, et al. Value of automatic bone subtraction in cranial CT angiography: comparison of bone-subtracted vs. standard CT angiography in 100 patients. *Eur Radiol*. 2008;18:974–982.
33. Sommer WH, Johnson TR, Becker CR, et al. The value of dual-energy bone removal in maximum intensity projections of lower extremity computed tomography angiography. *Invest Radiol*. 2009;44:285–292.
34. Behrendt FF, Schmidt B, Plumhans C, et al. Image fusion in dual energy computed tomography: effect on contrast enhancement, signal-to-noise ratio and image quality in computed tomography angiography. *Invest Radiol*. 2009;44:1–6.
35. Hein PA, Romano VC, Lembcke A, et al. Initial experience with a chest pain protocol using 320-slice volume MDCT. *Eur Radiol*. 2009;19:1148–1155.

7. Publikationen:

1. Saving dose in triple-rule-out computed tomography examination using a high-pitch dual spiral technique. Invest Radiol. 2010 Feb;45(2):64-71.

2. Dual energy CT of the chest: how about the dose? Invest Radiol. 2010 Jun;45(6):347-53

3. Feasibility and radiation dose of high-pitch acquisition protocols in patients undergoing dual-source cardiac CT. AJR Am J Roentgenol. 2010 Dec;195(6):1306-12

4. Systolic acquisition of coronary dual-source computed tomography angiography: feasibility in an unselected patient population. Eur Radiol. 2010 Jun;20(6):1331-6. Epub 2009 Dec 23.

8. Danksagung

An erster Stelle Danke ich selbstverständlich meinem Doktorvater PD Dr. med Thorsten Johnson sowie meinem Betreuer Dr. med Wieland Sommer für die hervorragenden Forschungsbedingungen und die Möglichkeit diese Dissertation durchführen zu können. Ihre konstruktive Kritik und wertvollen Erfahrungen auf diesem wissenschaftlichen Gebiet hat das Gesamtergebnis dieser Arbeit maßgeblich beeinflusst und mein Interesse an der Forschung in diesem spannenden Fachbereich der Medizin geweckt.

Ebenso gilt mein Dank allen Mitarbeitern des Instituts für klinische Radiologie sowie des Instituts für Strahlentherapie für ihre produktive und freundschaftliche Zusammenarbeit. Insbesondere möchte ich an dieser Stelle bei Herrn Neumaier, Frau Lechel und Frau Michalski für die tatkräftige technische Unterstützung bedanken.

Der mit Abstand wichtigste Dank geht an meine Eltern Axel und Ingrid für ihre unermüdliche Unterstützung und ihren stetigen Glauben an mich während des gesamten Studiums und der Erstellung dieser Promotion. Ohne sie wären meine Ausbildung und diese Arbeit nicht möglich gewesen und ich bin für ihre Hilfe unendlich dankbar. Ein ebenso wichtiger Dank geht an meine Frau Elisa, die immer für mich da ist und mich bei der Fertigstellung der Arbeit in jeglicher Hinsicht unterstützt hat.

9. Literaturverzeichnis

1. Lechel, U., et al., *Dose reduction by automatic exposure control in multidetector computed tomography: comparison between measurement and calculation.* Eur Radiol, 2009. **19**(4): p. 1027-34.
2. Einstein, A.J., et al., *Radiation dose and cancer risk estimates in 16-slice computed tomography coronary angiography.* J Nucl Cardiol, 2008. **15**(2): p. 232-40.
3. Brenner, D.J. and E.J. Hall, *Computed tomography--an increasing source of radiation exposure.* N Engl J Med, 2007. **357**(22): p. 2277-84.
4. Avrin, D.E., A. Macovski, and L.E. Zatz, *Clinical application of Compton and photo-electric reconstruction in computed tomography: preliminary results.* Invest Radiol, 1978. **13**(3): p. 217-22.
5. Johnson, T.R., et al., *Dual-source CT for chest pain assessment.* Eur Radiol, 2008. **18**(4): p. 773-80.
6. Coche, E., et al., *Diagnosis of acute pulmonary embolism in outpatients: comparison of thin-collimation multi-detector row spiral CT and planar ventilation-perfusion scintigraphy.* Radiology, 2003. **229**(3): p. 757-65.
7. Johnson, T.R., et al., *Material differentiation by dual energy CT: initial experience.* Eur Radiol, 2007. **17**(6): p. 1510-7.
8. Johnson, T.R., et al., *Diagnostic accuracy of dual-source computed tomography in the diagnosis of coronary artery disease.* Invest Radiol, 2007. **42**(10): p. 684-91.
9. Graser, A., et al., *Dual energy CT characterization of urinary calculi: initial in vitro and clinical experience.* Invest Radiol, 2008. **43**(2): p. 112-9.
10. Chae, E.J., et al., *Xenon ventilation CT with a dual-energy technique of dual-source CT: initial experience.* Radiology, 2008. **248**(2): p. 615-24.
11. Fink, C., et al., *Dual-Energy CT Angiography of the Lung in Patients with Suspected Pulmonary Embolism: Initial Results.* Rofo, 2008.
12. Goo, H.W., et al., *Xenon ventilation CT using a dual-source dual-energy technique: dynamic ventilation abnormality in a child with bronchial atresia.* Pediatr Radiol, 2008. **38**(10): p. 1113-6.
13. Morhard, D., et al., *Cervical and cranial computed tomographic angiography with automated bone removal: dual energy computed tomography versus standard computed tomography.* Invest Radiol, 2009. **44**(5): p. 293-7.
14. Scheffel, H., et al., *Dual-energy contrast-enhanced computed tomography for the detection of urinary stone disease.* Invest Radiol, 2007. **42**(12): p. 823-9.
15. Stolzmann, P., et al., *In vivo identification of uric acid stones with dual-energy CT: diagnostic performance evaluation in patients.* Abdom Imaging, 2009.

16. Thieme, S.F., et al., *Dual energy CT for the assessment of lung perfusion-Correlation to scintigraphy.* Eur J Radiol, 2008. **68**(3): p. 369-74.
17. Zhang, Y., et al., *[Radiological features of dual-energy CT lung perfusion imaging in patients with acute pulmonary embolism: comparison with CT pulmonary angiography].* Zhongguo Yi Xue Ke Xue Yuan Xue Bao, 2009. **31**(2): p. 166-70.
18. Bamberg, F., et al., *Diagnostic image quality of a comprehensive high-pitch dual-spiral cardiothoracic CT protocol in patients with undifferentiated acute chest pain.* Eur J Radiol.
19. Johnson, T.R., et al., *Optimization of contrast material administration for electrocardiogram-gated computed tomographic angiography of the chest.* J Comput Assist Tomogr, 2007. **31**(2): p. 265-71.
20. Johnson, T.R., et al., *[Dual-source CT in chest pain diagnosis].* Radiologe, 2007. **47**(4): p. 301-9.
21. Johnson, T.R., et al., *ECG-gated 64-MDCT angiography in the differential diagnosis of acute chest pain.* AJR Am J Roentgenol, 2007. **188**(1): p. 76-82.
22. Thieme, S.F., et al., *Dual Energy CT lung perfusion imaging-Correlation with SPECT/CT.* Eur J Radiol.
23. Thieme, S.F., et al., *Pulmonary ventilation and perfusion imaging with dual-energy CT.* Eur Radiol. **20**(12): p. 2882-9.
24. Thieme, S.F., et al., *Dual-energy CT for the assessment of contrast material distribution in the pulmonary parenchyma.* AJR Am J Roentgenol, 2009. **193**(1): p. 144-9.
25. Schenzle, J.C., et al., *Dual energy CT of the chest: how about the dose?* Invest Radiol. **45**(6): p. 347-53.
26. Sommer, W.H., et al., *Saving dose in triple-rule-out computed tomography examination using a high-pitch dual spiral technique.* Invest Radiol. **45**(2): p. 64-71.